Geoscience Frontiers 14 (2023) 101462

HOSTED BY

Contents lists available at ScienceDirect

Geoscience Frontiers

journal homepage: www.elsevier.com/locate/gsf

Research Paper

Lithospheric dripping in a soft collision zone: Insights from late Paleozoic magmatism suites of the eastern Central Asian Orogenic Belt

Zheng Ji [a,b], Wen-Chun Ge [b,*], M. Santosh [c,d], Chuan-Biao Wan [e], Yan-Long Zhang [b], Jun-Hui Bi [f], Hao Yang [b], Yu Dong [b], Yan Jing [b]

[a] College of Geo-exploration Science and Technology, Jilin University, Changchun 130026, China
[b] College of Earth Sciences, Jilin University, Changchun 130061, China
[c] School of Earth Science and Resources, China University of Geosciences, Beijing, Beijing 100083, China
[d] Department of Earth Sciences, University of Adelaide, Adelaide, South Australia 5005, Australia
[e] Exploration and Development Research Institute, Daqing Oilfield Limited Company, Daqing 163712, China
[f] Tianjin Center, China Geological Survey, Tianjin 300170, China

ARTICLE INFO

Article history:
Received 28 March 2022
Revised 30 July 2022
Accepted 24 August 2022
Available online 30 August 2022
Handling Editor: V.O. Samuel

Keywords:
Soft collision
Lithospheric dripping
Double-sided subduction
Central Asian Orogenic Belt
Late Paleozoic

ABSTRACT

The closure of Paleo-Asian Ocean is considered to have occurred along the Solonker Suture in the southernmost segment of the Central Asian Orogenic Belt (CAOB), the largest Phanerozoic accretionary orogen on the globe. The suture branches to the east to form the northern Hegenshan–Heihe Suture and the southern Solonker–Changchun Suture. The Hegenshan–Heihe Suture is an ideal natural laboratory for studying the post-collisional geodynamic processes operating in a soft collision zone driven by divergent double-sided subduction. Here we report results from an integrated study of the petrology, geochronology, geochemistry, and Sr–Nd–Hf isotopic compositions of the Early Carboniferous–Early Permian magmatic suite in the Hailar Basin of the Xing'an–Erguna Block. The Early Carboniferous igneous rocks are represented by 356–349 Ma andesitic tuffs, exhibiting typical subduction-related features, such as enrichment in large-ion lithophile elements and depletion in high-field-strength elements. These features, together with the relatively depleted Sr–Nd–Hf isotopic compositions, constant Nb/Y values, but highly variable Rb/Y and Ba values indicate that these rocks were generated by partial melting of a depleted mantle wedge metasomatized by slab-derived fluids. The Late Carboniferous–Early Permian magmatic suite (317–295 Ma) is characterized by high Sr contents (313–1080 ppm) and low Y contents (5–13 ppm), and these can be subdivided into calc-alkaline adakitic rocks and high-K calc-alkaline adakitic rocks. The calc-alkaline adakitic rocks have higher values of Sr/Y, $(Sm/Yb)_{source\ normalized}$, and Mg#, and lower values of Y, $Yb_{source\ normalized}$, and K_2O/Na_2O than the high-K calc-alkaline adakitic rocks, which suggests that the former was generated by partial melting of foundered lower continental crust and the latter by partial melting of normal lower continental crust. Based on our new data, in conjunction with those in previous studies, we conclude that the tectonic evolution of the Hegenshan–Heihe Suture involved Early Carboniferous double-sided subduction of the Nenjiang Ocean, latest Early Carboniferous soft collision between the Xing'an–Erguna and Songliao blocks, and Late Carboniferous–Early Permian post-collisional extension. We also propose a new geodynamic scenario in which removal of the lithospheric root might have occurred in a soft collision zone during the post-collision period via repeated and localized lithospheric dripping, which results from combined effects of hydration weakening of the lithosphere caused by pre-collision subduction and asthenospheric stirring triggered by slab break-off.

1. Introduction

Closure of ocean basin and subsequent continental collision are integral components of the Wilson cycle (Wilson, 1966), which are significant not only for the formation of orogenic systems, but also

* Corresponding author at: College of Earth Sciences, Jilin University, Changchun 130061, China.
E-mail address: gewenchun@jlu.edu.cn (W.-C. Ge).

https://doi.org/10.1016/j.gsf.2022.101462

for the recycling of crustal materials into the mantle. Two distinct geodynamic processes have been identified during the closure of ocean basins and continental collision (Frisch et al., 2011; Zhao, 2015; Zhu et al., 2016). The first involves classic single-sided oceanic subduction where oceanic lithosphere is subducted beneath continental lithosphere on one side of the oceanic plate and is directly connected with the passive margin of another continent on the other side (Yin and Harrison, 2000; Compagnoni, 2003). The result is the development of a single magmatic arc on the overriding continental plate. When the oceanic lithosphere has been totally consumed by subduction, the passive continental margin is dragged beneath the other continent by the subducted oceanic slab, and the two continents hard collide and weld together (Hacker et al., 2000; Zheng et al., 2003). The result of such a hard

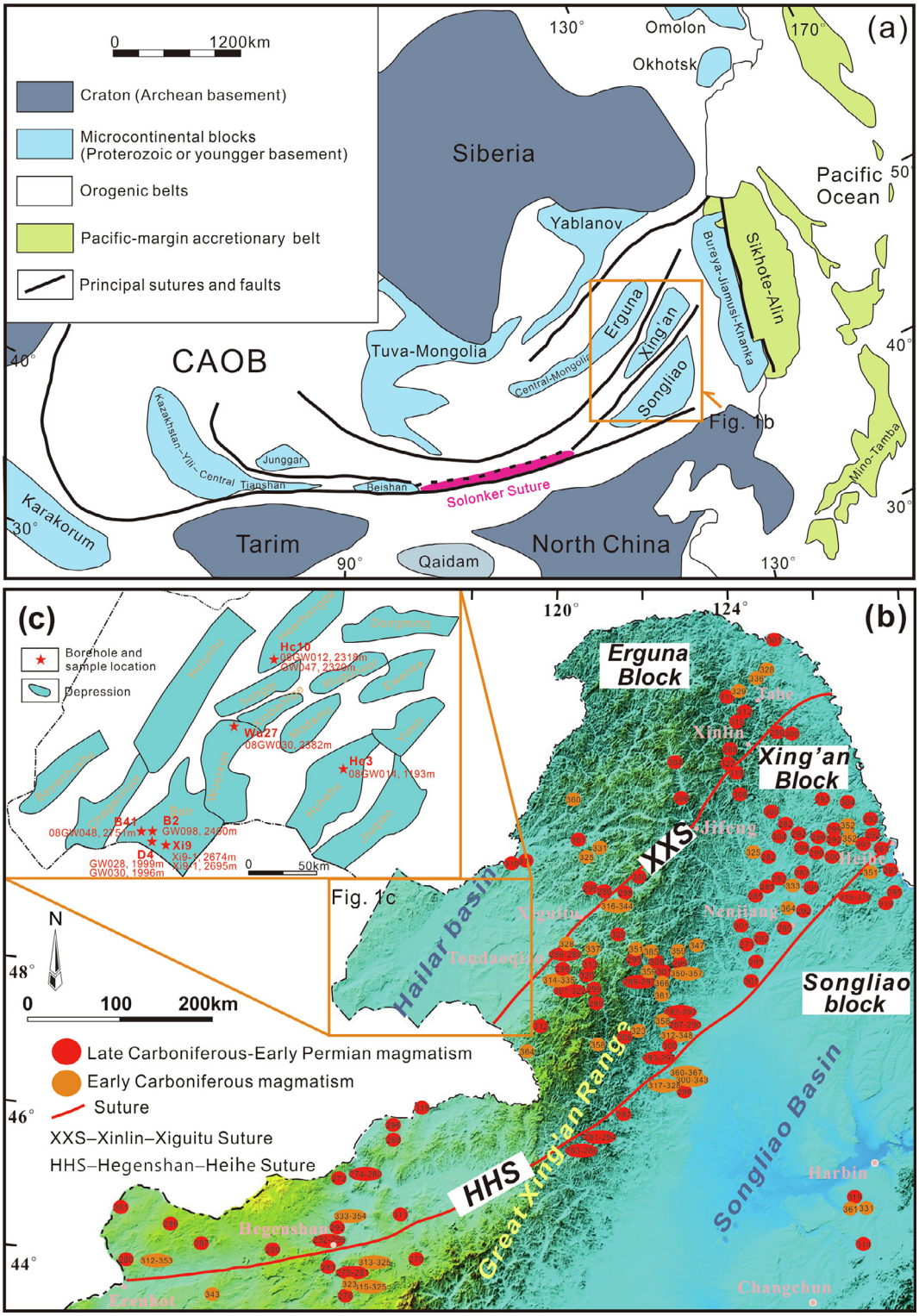

Fig. 1. (a) Schematic tectonic map showing the division of central and eastern Asia (after Zhou et al., 2017). (b) Tectonic division of NE China (after Liu et al., 2017). (c) Distribution of the Early Carboniferous–Early Permian magmatic ages in the Xing'an–Erguna Block and adjacent areas (after Liu et al., 2021). Age data are from Liu et al. (2021) and references therein.

collision is significant crustal thickening, the development of fold and thrust structures, and high-grade metamorphism (Hacker et al., 2000; Yin and Harrison, 2000; Compagnoni, 2003; Zheng et al., 2003; Song et al., 2015a). The second process involves divergent double-sided oceanic subduction where an oceanic lithosphere is subducted at both sides of the plate, generating two magmatic arcs on the opposing overriding plates (Soesoo et al., 1997; Xiao et al., 2003; Eizenhöfer et al., 2015; Zhao, 2015). Unlike single-sided oceanic subduction, the drag force of subducted oceanic lithosphere disappears as oceanic lithosphere and continental lithosphere remain separated in double-sided oceanic subduction (Song et al., 2015a; Zhao, 2015). Thus, if the two continents collide, they weld together through a process of soft collision, without the involvement of continental deep subduction, ultrahigh-pressure metamorphism, or well-developed fold–thrust structures (Eizenhöfer et al., 2015; Song et al., 2015b; Eizenhöfer and Zhao, 2018). It is well acknowledged that hard collision is generally accompanied by removal of the orogenic root as a result of lithospheric delamination (e.g., in the Cenozoic Himalayan collisional orogeny; Turner et al., 1996; Chung et al., 2005), which induces extensive post-collisional magmatism. However, it remains unclear whether and, if any, how the root would be removed after a soft collision without continental deep subduction and a strong orogeny (Xiao et al., 2003; Song et al., 2015a).

The Central Asian Orogenic Belt (CAOB) is the largest Phanerozoic accretionary orogen in the world and is situated between the Siberian and Baltica cratons to the north and the Tarim and North China cratons to the south (Sengör et al., 1993; Jahn et al., 2004; Windley et al., 2007; Fig. 1a). Its tectonic evolution was characterized by the amalgamation of island arcs, ophiolites, oceanic islands, seamounts, accretionary wedges, oceanic plateaus, and microcontinents in association with the progressive closure of the Neoproterozoic to early Mesozoic Paleo-Asian Ocean following the breakup of Rodinia and until the assembly of Pangea (Xiao et al., 2003; Wu et al., 2011; Xiao and Santosh, 2014; Zhou et al., 2018; Liu et al., 2021). Although the main oceanic basins of the Paleo-Asian Ocean in the archipelagic pattern of the CAOB remain contentious, it is generally accepted that the growth of the CAOB migrated southwards with the Paleo-Asian Ocean ultimately closing along the Solonker Suture in the southernmost section of the CAOB (Eizenhöfer and Zhao, 2018; Xiao et al., 2020). The Solonker Suture is named after its type locality of ophiolitic rock outcrops that straddle the southernmost Chinese–Mongolian border, and the suture separates the Mongolian Terrane to the northwest from the North China Craton to the southeast (Xiao et al., 2003; Eizenhöfer et al., 2015; Eizenhöfer and Zhao, 2018). The suture branches to the east to form the northern Hegenshan–Heihe Suture and the southern Solonker–Changchun Suture, both of which have attracted significant attention due to their importance in understanding the final stages of evolution of the eastern Paleo-Asian Ocean and major late Paleozoic to early Mesozoic collisional orogenic processes in the southeastern section of the CAOB (Xiao et al., 2003; Liu et al., 2017; Ji et al., 2018; Eizenhöfer and Zhao, 2018; Yang et al., 2019; Jing et al., 2020; Lu et al., 2020). It was previously thought that the Hegenshan–Heihe Suture resulted from the closure of the Nengjiang Ocean (a northern branch of the eastern Paleo-Asian Ocean) via westward subduction during the late Paleozoic (Li et al., 2014; Feng et al., 2015; Liu et al., 2017; Zhang et al., 2018). However, deep reflection seismic profiles showed that there is an east-dipping strong reflection interface in the deep part of the western margin of the Songliao Basin extending to the Moho surface, indicating the eastward subduction of the Nenjiang Ocean (Hou et al., 2015; Liu et al., 2019). Moreover, recent studies indicate the existence of Early Carboniferous magmatic arc assemblages on both sides of the suture (Zhao et al., 2010; Zhang et al., 2018; Ma et al., 2019; Ma et al., 2020a), suggesting that the Nengjiang Ocean between the Xing'an–Erguna Block (XEB) and the Songliao Block (SB) underwent divergent double-sided subduction (Ma et al., 2020a; Liu et al., 2019; Liu et al., 2021). The absence of unambiguous collision-related regional features along the Hegenshan–Heihe Suture (e.g., high-grade regional metamorphism, well-developed fold–thrust structures, regionally coherent ophiolite belts) further confirms that a soft collision between the XEB and SB took place after the closure of the Nengjiang Ocean, similar to that along the Solonker–Changchun Suture (Eizenhöfer and Zhao, 2018; Ma et al., 2019; Ma et al., 2020a). Thus, the Hegenshan–Heihe Suture is an ideal natural laboratory for studying the post-collisional geodynamic processes operating in a soft collision zone driven by divergent double-sided subduction. The XEB is characterized by widespread Early Carboniferous–Early Permian magmatism, which is generally accepted to be the result of late-stage subduction of the Nengjiang oceanic lithosphere and subsequent continental collision/post-collision processes (Wu et al., 2011; Dong et al., 2016; Zhang et al., 2018; Guo et al., 2019; Yang et al., 2019; Li et al., 2020). This area therefore provides an excellent window to investigate the s late-stage tectonomagmatic evolution of the Hegenshan–Heihe Suture.

In this study, we present zircon U–Pb ages and Lu–Hf isotopic compositions, as well as whole-rock geochemical and Sr–Nd isotopic data for the Early Carboniferous–Early Permian igneous rocks in the XEB. These new results are employed to evaluate the petrogenesis of these rocks, as well as to reconstruct the processes of transition from oceanic subduction to continental collision in the area. In conjunction with published informatoin, we propose a new geodynamic scenario which envisages the removal of a lithospheric root in a soft collision zone during the post-collision period in the form of repeated and localized lithospheric dripping, which results from hydration weakening of lithosphere caused by pre-collision subduction and asthenospheric stirring triggered by slab break-off.

2. Geological setting and sample descriptions

The CAOB is a huge orogenic collage that is subdivided into a western segment containing the Kazakhstan–Yili–Central Tianshan and Junggar blocks, a central segment containing the Tuva–Mongolia and Beishan blocks, and an eastern segment containing the combined northeastern(NE) China blocks (Wu et al., 2011; Xiao and Santosh, 2014; Zhou et al., 2018; Fig. 1a). The NE China segment of the CAOB, also known as Xing'an–Mongolian Orogenic Belt (XMOB), consists of a collage of microcontinental blocks/accretionary terranes that were accreted to the margins of the Siberian and North China cratons (Xu et al., 2015; Liu et al., 2017). The Palaeozoic tectonic evolution of NE China was dominated by the closure of the Paleo-Asian Ocean, which led to amalgamation of multiple blocks (i.e., Erguna, Xing'an, Songliao blocks) (Wu et al., 2011). Younger tectonomagmatic events in NE China were related to the Mesozoic subduction of the Paleo-Pacific Plate, which resulted in the accretion of circum-Pacific orogenic terranes (i.e., Jiamusi–Khanka and Nadanhada blocks) (Zhou and Li, 2017; Ji et al., 2019a).

The Erguna Block (EB), located in the westernmost region of NE China (Fig. 1b), is bounded to the northwest by the Mesozoic Mongolia–Okhotsk Suture and to the southeast by the early Paleozoic Xinlin–Xiguitu Suture (Zhou et al., 2018). The Precambrian basement rocks, represented by Neoarchean–Proterozoic gneissic granitoids (ca. 2600–700 Ma) and Neoproterozoic metamorphic supracrustal rocks (e.g., Xinhuadukou, Ergunahe, and Jiageda groups), are well preserved in the northwestern part of the EB (Ge et al., 2015; Tang et al., 2013; Zhou et al., 2018; Liu et al., 2021). The Phanerozoic strata are dominated by the Paleozoic

shallow marine sandstones and Mesozoic volcanic and sedimentary rocks (IMBGMR, 1991). Meanwhile, Phanerozoic granitoids are widespread throughout the EB, which were mostly emplaced during the Early Jurassic–Late Triassic (220–182 Ma), with lesser magmatism occurred during the Early Cretaceous (132–118 Ma), Late Carboniferous–Permian (336–250 Ma), and Middle Cambrian–Early Devonian (517–416 Ma) (Wu et al., 2011).

The Xing'an Block (XB) is located adjacent to the southeast of the EB and composed mainly of Palaeozoic granitoids and sedimentary strata covered/cut by large volumes of Mesozoic volcanic rocks and granitoids. It is traditionally thought that Precambrian basement rocks (i.e., Xinghuadukou, Xinkailing, Luomahu, Wolegen, and Zhalantun groups and Ergunahe and Jiageda formations) are sporadically distributed in this block (IMBGMR, 1991). However, new zircon U–Pb age data have confirmed that the so-called Precambrian rocks in the XB are mainly early to late Paleozoic with less early Mesozoic rock associations, which cannot be taken as Precambrian basement (Miao et al., 2007; Sun et al., 2014). Thus, some scholars doubt that Precambrian metamorphic basement might not exist in the XB (Wu et al., 2011; Liu et al., 2017), although a few detrital zircons from the metasedimentary rocks in the Zhalantun and Duobaoshan areas have ages varying from 2952 Ma to 566 Ma (Zhou et al., 2018). Based on the recognition of 697–539 Ma Ali–Xinlin ophiolitic rocks (Feng et al., 2016, 2018a), 510–490 Ma Toudaoqiao blueschists (Zhou et al., 2015), and 494–480 Ma Tahe–Huma post-collisional plutons (Ge et al., 2005; Feng et al., 2017), amalgamation of the EB and XB was commonly believed to have completed before ca. 490 Ma. Subsequently, a Late/Mddile Ordovician–Silurian arc–back-arc system developed in the integrated XEB as a result of westward subduction of the Nenjiang oceanic plate (Feng et al., 2018a; Liu et al., 2021).

The SB is bounded by the XB to the northwest and the Jiamusi–Khanka Block to the east, separated by the Hegenshan–Heihe Suture and Heilongjiang Complex, respectively. Main body of the SB is covered by the Songliao Basin with thick filling of late Mesozoic–Cenozoic sediments (Ji et al., 2019b). Data from several hundred drill holes revealed that the basement beneath the Songliao Basin is mainly composed of deformed and metamorphosed Palaeozoic–Mesozoic granitoids and Palaeozoic volcanic–sedimentary strata, but no Precambrian rocks have been identified within the basin basement (Wu et al., 2001; Wu et al., 2011). Notably, some Precambrian ages have been reported in the periphery of the Songliao Basin, including the ca. 2.6 Ga trondhjemites and ca. 1.8 Ga A-type granite in the Longjiang area (Qian et al., 2018; Zhang et al., 2018), ca. 1.8 Ga deformed intrusive rocks in the Gongzhuling area (Pei et al., 2007), and ca. 929–841 Ma granitoids in the Yichun area (Luan et al., 2019). Recently, a NE-oriented Early Carboniferous magmatic arc has been recognized along the western margin of the SB, indicates the eastward subduction of the Nenjiang oceanic plate have happened beneath the SB (Ma et al., 2020a; Liu et al., 2021).

In this study, representative samples of the Early Carboniferous–Early Permian magmatic rocks were collected from seven drill holes (i.e., Xi9, Wu27, D4, B2, B41, H3, and Hc10) in the Hailar Basin that is developed on the XEB. Details of the locations (including well locations and depth) of samples are provided in Fig. 1c. The lithologies include mainly rhyolites, dacites, andesites, andesitic tuffs, and monzogranites, and all of these samples are described below. The rhyolites show massive structure and porphyritic texture and contain 5%–10% phenocrysts of alkali feldspar, plagioclase, and quartz in a groundmass of aphanitic felsic minerals and glass (Supplementary data Fig. S1a). The dacites display porphyritic and pilotaxitic textures (Supplementary data Fig. S1b). Their phenocrysts are dominated by plagioclase, along with minor quartz and amphibole. The andesites are massive and porphyritic with 30%–35% phenocrysts of plagioclase and amphibole in a hyalopilitic groundmass of microcrystalline plagioclase and volcanic glass (Supplementary data Fig. S1c and d). The andesitic tuffs have a massive structure and a tuffaceous texture and consist of crystal clasts (plagioclase, amphibole, and pyroxene; 65%–70%), volcanic dusts (20%–25%), and vitroclasts (5%–10%) (Supplementary data Fig. S1e). The monzogranites display medium–fine-grained subhedral textures and consist of plagioclase (35%–45%), alkali feldspar (25%–30%), quartz (20%–25%), biotite (~5%), and minor accessory minerals of zircon, magnetite, and apatite (Supplementary data Fig. S1f).

3. Analytical results

The detailed methods for zircon U–Pb dating and geochemical analyses (major elements, trace elements, and Sr–Nd–Hf isotopes) are described in the Supplementary data, Text S1.

3.1. Zircon U–Pb ages and Hf isotopic compositions

The zircon U–Pb and Lu–Hf isotopic compositions for ten late Paleozoic igneous rock samples from the Hailar Basin are presented in Supplementary data Table S1 and S2, respectively. The zircon grains analyzed for this study exhibit typical characteristics of igneous zircons (e.g., clear oscillatory zoning, euhedral to subhedral shapes, high Th/U ratios), indicating an igneous origin.

Two samples of andesitic tuff (Xi9-1 and Xi9-2) were collected from borehole Xi9 at depths of 2694.44 m and 2695.29 m, respectively. Both samples have been dated by Meng et al. (2013) using LA–ICP–MS zircon U–Pb methods and yield formation ages of 356 ± 5 Ma (MSWD = 0.60) and 349 ± 5 Ma (MSWD = 1.80) (Fig. 2a and b), respectively. In this study, a total of 15 Lu–Hf isotope analyses were conducted on 15 magmatic zircons from sample Xi9-1, yielding $^{176}Hf/^{177}Hf$ ratios of 0.282882–0.283008 and $\varepsilon_{Hf}(t)$ values of +11.54 to +15.77. Nineteen Lu–Hf isotope analyses were conducted on 19 magmatic zircons from sample Xi9-2, yielding $^{176}Hf/^{177}Hf$ ratios of 0.282890–0.282960 and $\varepsilon_{Hf}(t)$ values of +11.68 to +14.01 (Fig. 3).

Rhyolite sample 08GW030 was collected from borehole Wu27 at a depth of 2382.55 m. A total of 22 zircons from this sample were analyzed. Fourteen zircons have $^{206}Pb/^{238}U$ ages of 319–314 Ma, yielding a weighted mean $^{206}Pb/^{238}U$ age of 317 ± 10 Ma (MSWD = 0.01) (Fig. 2c), which represents formation age of the rhyolite. Eight zircons record older ages of 1394–355 Ma, which are interpreted as crystallization ages of captured zircons. Fourteen Lu–Hf isotope analyses were conducted on 14 magmatic zircons, yielding $^{176}Hf/^{177}Hf$ ratios of 0.282778–0.282937 and $\varepsilon_{Hf}(t)$ values of +6.67 to +12.51 (Fig. 3).

Andesite sample GW028 and dacite sample GW030 were collected from borehole D4 at depths of 1999.42 m and 1996.65 m, respectively. Both samples have been dated by Meng et al. (2013) using LA–ICP–MS zircon U–Pb methods and yield formation ages of 315 ± 4 Ma (MSWD = 0.30) and 298 ± 3 Ma (MSWD = 1.20) (Fig. 2d and e), respectively. In this study, a total of 17 Lu–Hf isotope analyses were conducted on 17 magmatic zircons from the sample GW028, yielding $^{176}Hf/^{177}Hf$ ratios of 0.282870–0.283028 and $\varepsilon_{Hf}(t)$ values of +10.16 to +15.76. Twelve Lu–Hf isotope analyses were conducted on 12 magmatic zircons from sample GW030, yielding $^{176}Hf/^{177}Hf$ ratios of 0.282860–0.283011 and $\varepsilon_{Hf}(t)$ values of +9.50 to +14.87 (Fig. 3).

Dacite sample GW098 was collected from borehole B2 at a depth of 2400.60 m. The sample has been dated by Meng et al. (2013) using LA–ICP–MS zircon U–Pb methods and yields a formation age of 295 ± 3 Ma (MSWD = 0.60) (Fig. 2f). In this study, a total of 9 Lu–Hf isotope analyses were conducted on 9 magmatic zircons

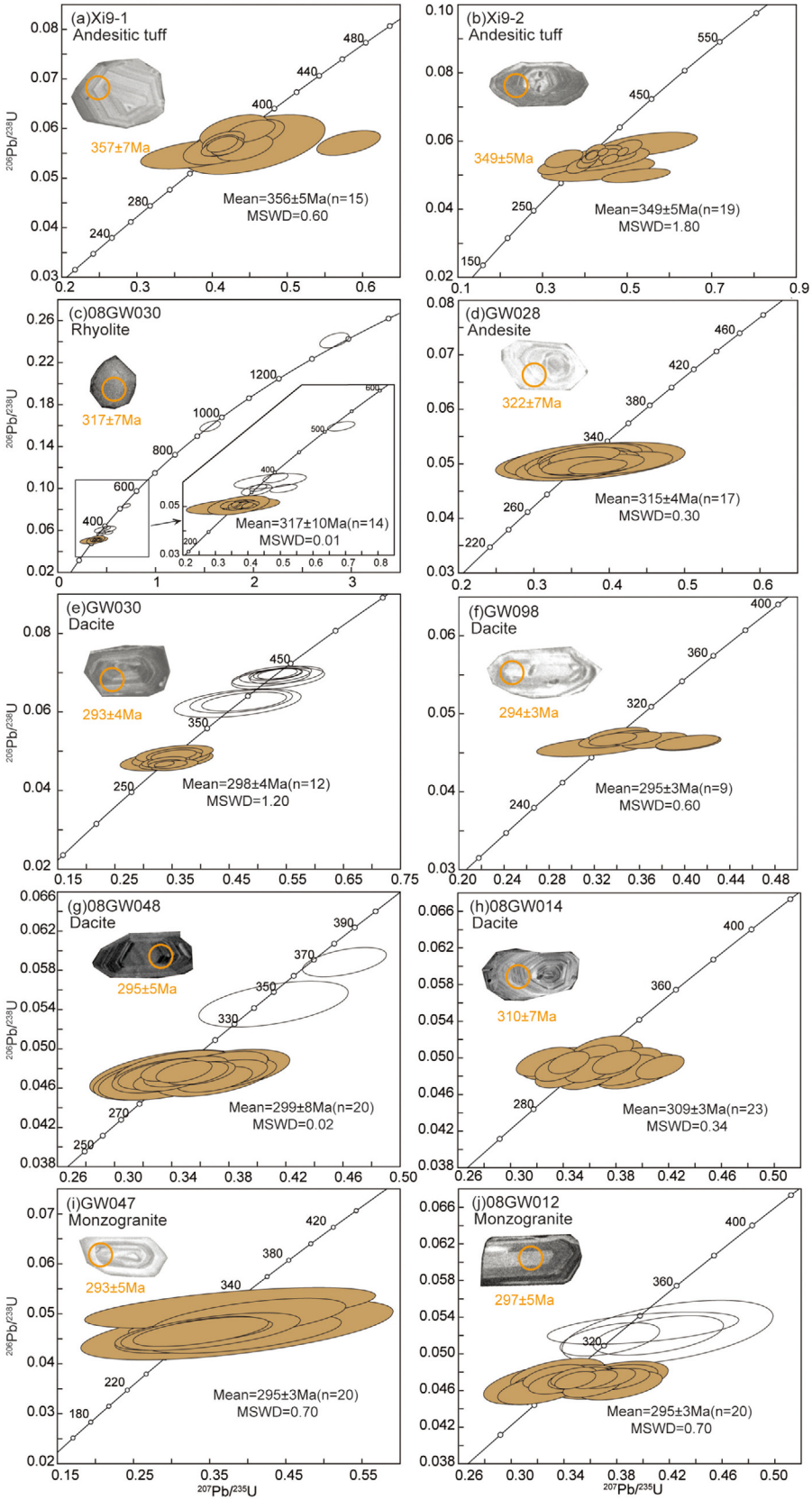

Fig. 2. Zircon U–Pb concordia diagrams of the Early Carboniferous–Early Permian igneous rocks in the Hailar Basin (samples GW028, GW030, GW047, GW098, Xi9-1, and Xi9-2 from Meng et al., 2013).

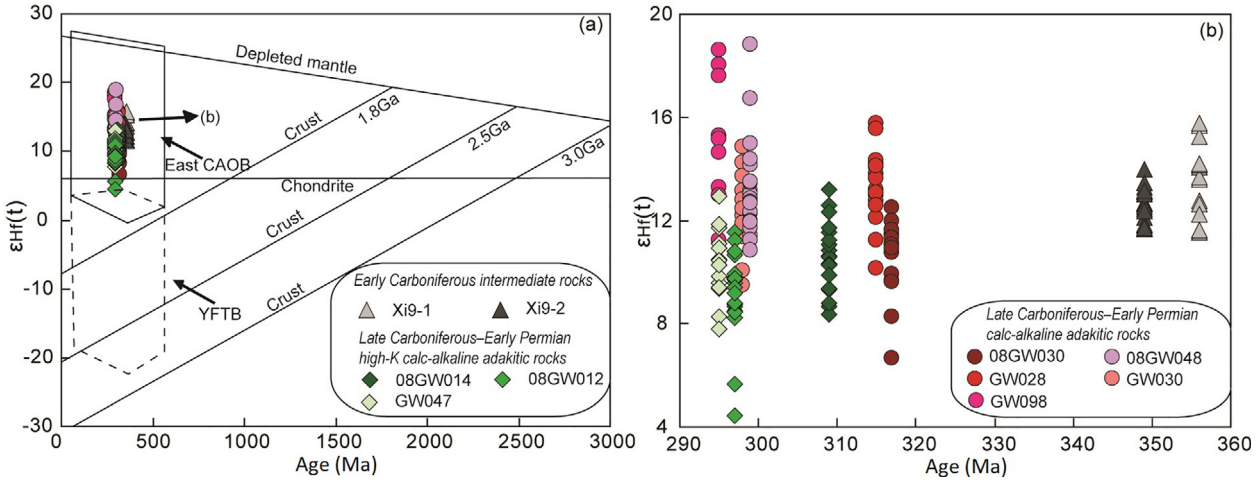

Fig. 3. (a) Zircon $\varepsilon_{Hf}(t)$ vs U–Pb age diagram for the Early Carboniferous–Early Permian igneous rocks in the Hailar. CAOB = Central Asian Orogenic Belt; YFTB = Yanshan Fold-and-Thrust Belt (ranges for the East CAOB and YFTB are from Yang et al., 2006). (b) Close-up view of the distribution of samples in the $\varepsilon_{Hf}(t)$ vs. T diagram shown in Fig. 3a.

from the sample, yielding $^{176}Hf/^{177}Hf$ ratios of 0.282913–0.283126 and $\varepsilon_{Hf}(t)$ values of +11.26 to +18.60 (Fig. 3).

Dacite sample 08GW048 was collected from borehole B41 at a depth of 2751.28 m in the Beir Depression. A total of 22 U–Pb isotope analyses were performed on 22 zircons. Two zircons with ages of 369 Ma and 342 Ma are interpreted as xenocrysts. The remaining 20 zircons yield a weighted mean $^{206}Pb/^{238}U$ age of 299 ± 8 Ma (MSWD = 0.02) (Fig. 2g), representing formation age of the dacite. Twenty Lu–Hf isotope analyses were conducted on 20 magmatic zircons, yielding $^{176}Hf/^{177}Hf$ ratios of 0.282899–0.283126 and $\varepsilon_{Hf}(t)$ values of +10.85 to +18.81 (Fig. 3).

Dacite sample 08GW014 was collected from borehole He3 at a depth of 1193.70 m in the Huhehu Depression. Twenty-three U–Pb isotope analyses of zircons yield $^{206}Pb/^{238}U$ ages of 318–302 Ma and a weighted mean $^{206}Pb/^{238}U$ age of 309 ± 3 Ma (MSWD = 0.34) (Fig. 2h), representing formation age of the dacite. Twenty Lu–Hf isotope analyses of magmatic zircons yield $^{176}Hf/^{177}Hf$ ratios of 0.282821–0.282960 and $\varepsilon_{Hf}(t)$ values of +8.37 to +13.20.

Two samples of monzogranite (GW047 and 08GW012) were collected from borehole Hc10 at depths of 2320.10 m and 2318.00 m, respectively. Sample GW047 has been dated by Meng et al. (2013) using LA–ICP–MS zircon U–Pb method and yielded a formation age of 295 ± 3 Ma (MSWD = 0.70) (Fig. 2i). In this study, twenty-three U–Pb isotope analyses of zircons from sample 08GW012 yield two groups of weighted mean $^{206}Pb/^{238}U$ ages: 328 ± 8 Ma (MSWD = 0.22) and 297 ± 7 Ma (MSWD = 0.02) (Fig. 2j). The former represents crystallization age of the captured zircon, whereas the latter is interpreted as formation age of monzogranite. Fourteen Lu–Hf isotope analyses were conducted on 14 magmatic zircons from sample GW047, yielding $^{176}Hf/^{177}Hf$ ratios of 0.282819–0.282956 and $\varepsilon_{Hf}(t)$ values of +7.80 to +12.92. Ninteen Lu–Hf isotope analyses were conducted on 19 magmatic zircons from sample 08GW012, yielding $^{176}Hf/^{177}Hf$ ratios of 0.282720–0.282917 and $\varepsilon_{Hf}(t)$ values of +4.43 to +11.54 (Fig. 3).

3.2. Whole-rock major and trace elements

3.2.1. Early Carboniferous intermediate rocks

The Early Carboniferous intermediate rocks comprise the ca. 356 Ma and ca. 349 Ma andesitic tuffs from borehole Xi9. They have a restricted range of SiO_2 (54.94–56.86 wt.%), Al_2O_3 (16.24–17.12 wt.%), $Fe_2O_3^T$ (7.18–7.54 wt.%), MgO (3.54–3.92 wt.%), Na_2O (4.80–5.84 wt.%), and K_2O (1.80–2.02 wt.%) contents and Mg# values (48–51) (Supplementary data Table S3). The intermediate rocks plot within the trachyandesite and basaltic andesite fields in a total alkalis versus silica (TAS) diagram (Fig. 4a) and are classified as calc-alkaline series in a Th versus Co diagram (Fig. 4b). These rocks are moderately enriched in light rare earth elements (LREEs) [$(La/Yb)_N$ = 6.48–7.48] with weakly negative Eu anomalies (Eu/Eu^*=0.91–0.94) (Fig. 5a). In the primitive-mantle-normalized spidergram (Fig. 5b), they show enrichments in large-ion lithophile elements (LILEs; e.g., Ba, K, and Sr) and depletions in high-field-strength elements (HFSEs; e.g., Nb, Ta, and Ti).

3.2.2. Late Carboniferous–Early Permian intermediate-acidic rocks

The most remarkable feature of the Late Carboniferous–Early Permian intermediate-acidic rocks analysed in this study is their adakitic nature, characterized by high Sr contents (313–1080 ppm), low Y (5–13 ppm) and HREE (e.g., Yb = 0.41–1.44 ppm) contents, and resultant high Sr/Y (24–161) and $(La/Yb)_N$ (5–21) ratios (Fig. 4c). Although all the Late Carboniferous–Early Permian adakitic rocks belong to the subalkalic series in a TAS diagram (Fig. 4a), they can be subdivided into calc-alkaline adakitic rocks (include the ca. 317 Ma rhyolites from borehole Wu7, ca. 315–298 Ma andesites and dacites from borehole D4, ca. 299 Ma dacites from borehole B41, and ca. 295 Ma dacites from borehole B2) and high-K calc-alkaline adakitic rocks (include the ca. 309 Ma dacites from borehole He3 and ca. 297–295 Ma monzogranite from borehole Hc10) in a Th vs Co diagram (Fig. 4b).

The calc-alkaline adakitic rocks have variable SiO_2 (60.23–69.50 wt.%), high Na_2O (3.94–5.69 wt.%) and Al_2O_3 (15.39–17.00 wt.%), and moderate K_2O (2.36–2.95 wt.%) contents with moderate K_2O/Na_2O ratios (0.50–0.62). MgO and total Fe_2O_3 contents of the calc-alkaline adakitic rocks vary from 1.16 wt.% to 2.69 wt.% and 2.58 wt.% to 4.37 wt.%, respectively, corresponding to high Mg# values (47–55). Compared with the calc-alkaline adakitic rocks, the high-K calc-alkaline adakitic rocks show similar SiO_2 (65.72–67.37 wt.%) contents, but lower Na_2O (3.71–4.26 wt.%) and Al_2O_3 (14.19–15.70 wt.%) contents and Mg# values (41–47) and higher K_2O contents (3.01–3.39 wt.%) and K_2O/Na_2O ratios (0.72–0.90).

Both of these are characterized by obvious REE fractionation [$(La/Yb)_N$ = 5.16–19.40], insignificant Eu anomalies (Eu/Eu^* = 0.79–1.23), enrichments in LILEs, and depletions in HFSEs (Fig. 5c and d). However, in the Sr/Y vs Y diagram, high-K calc-alkaline adakitic rocks plot the overlapping field of adakites and normal arc magmatic rocks, whereas the calc-alkaline adakitic rocks have higher Sr/Y ratios and lower Y contents than the high-K calc-alkaline ones, plotting only within the adakite field (Fig. 4c).

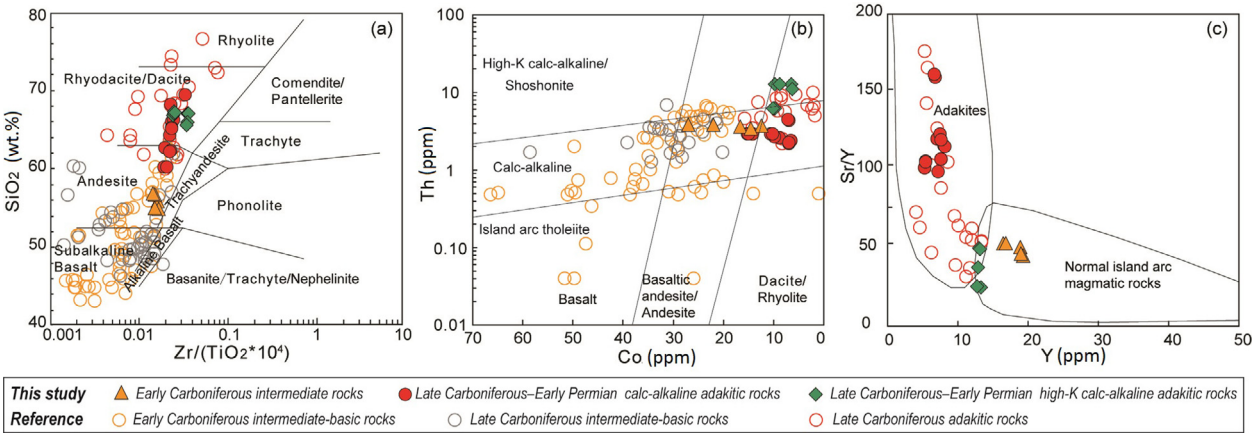

Fig. 4. Plots of (a) SiO_2 vs Zr/TiO_2 (after Winchester and Floyd, 1976), (b) Th vs Co (after Hastie et al., 2007), and (c) Sr/Y vs Y (after Defant and Drummond, 1990) for the Early Carboniferous–Early Permian igneous rocks in the Hailar Basin. Data for the Early Carboniferous intermediate–basic rocks in the Xing'an–Erguna Block are from Zhou et al. (2005), Zhao et al. (2010), Feng et al. (2018), Yu (2017), Dong et al. (2016), Zhang et al. (2018), and Li et al. (2020). Data for the Late Carboniferous intermediate–basic rocks in the Xing'an–Erguna Block are from Feng et al. (2014, 2015), Gou et al. (2018), Dong et al. (2020), and Yu (2017). Data for the Late Carboniferous adakitic rocks in the Xing'an–Erguna Block are from Ji et al. (2018), Zhang et al. (2010, 2016, 2018), and Zhao et al. (2010).

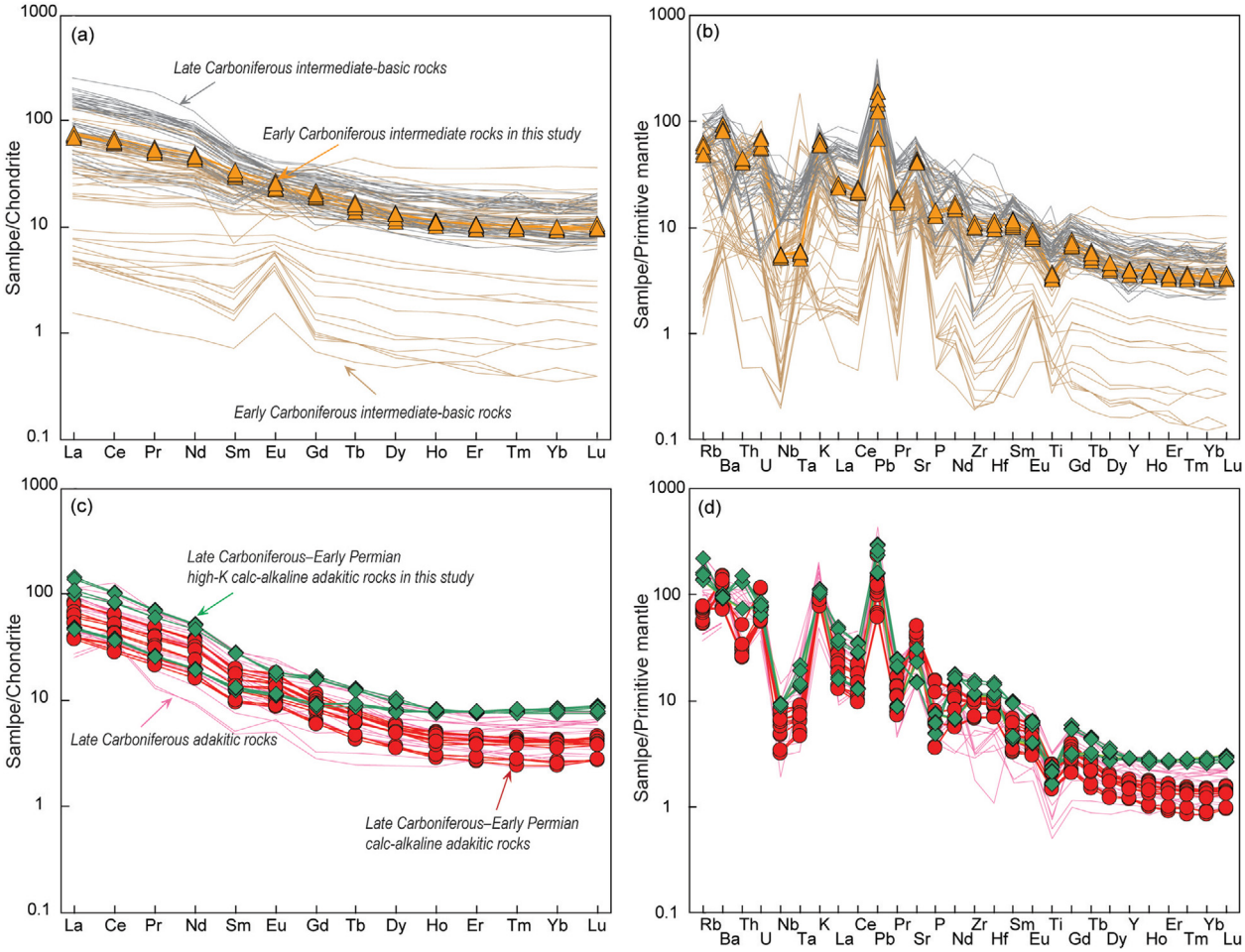

Fig. 5. Chondrite-normalized REE patterns (a,c) and primitive-mantle-normalized trace element spidergrams (b,d) for the Early Carboniferous–Early Permian igneous rocks in the Hailar Basin. Chondrite-normalized and primitive-mantle-normalized values are from Sun and McDonough (1989).

3.3. Whole-rock Sr–Nd isotopic compositions

Whole-rock Sr–Nd isotopic data of the studied Early Carboniferous–Early Permian igneous rocks are listed in Supplementary data Table S4. As shown in the plot of $\varepsilon_{Nd}(t)$ vs. $(^{87}Sr/^{86}Sr)_i$ (Fig. 6a), the Early Carboniferous intermediate rocks have depleted Sr–Nd isotopic compositions with $(^{87}Sr/^{86}Sr)_i$ ratios of 0.704732 to 0.704750 and $\varepsilon_{Nd}(t)$ values of +5.35 to +5.54. The Late Carboniferous–Early Permian high-K calc-alkaline adakitic rocks and calc-alkaline adakitic rocks have similar $(^{87}Sr/^{86}Sr)_i$ ratios (0.703781–

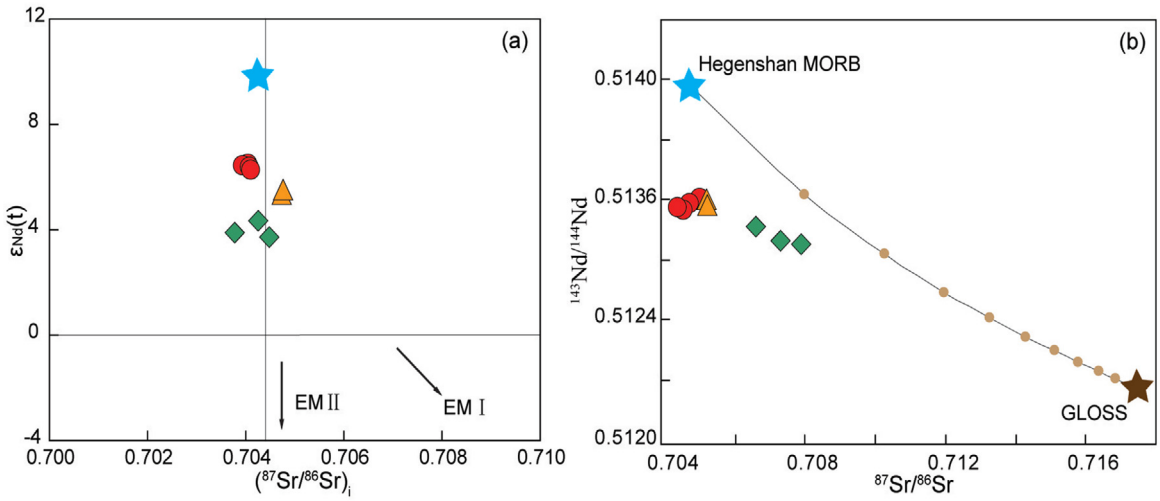

Fig. 6. Plots (a) $\varepsilon_{Nd}(t)$ vs $(^{87}Sr/^{86}Sr)_i$ and (b) $^{143}Nd/^{144}Nd$ vs $^{87}Sr/^{86}Sr$ for the Early Carboniferous–Early Permian igneous rocks in the Hailar Basin. Data for Hegenshan MORB and GLOSS are from Jian et al. (2012) and Plank and Langmuir (1998), respectively. Symbols are the same as those in Fig. 5.

0.704465), but the $\varepsilon_{Nd}(t)$ values of the calc-alkaline adakitic rocks (+6.28 to +6.48) are higher than those of the high-K calc-alkaline adakitic rocks (+3.72 to +4.33).

4. Discussion

4.1. Petrogenesis

4.1.1. Alteration effects

The late Paleozoic igneous rock samples from the Hailar Basin show various degrees of alteration, as indicated by their LOI values (0.98–5.43 wt.%). It is therefore crucial to evaluate the possible effects of alteration on the geochemical compositions of these rocks. The lack of correlations between LOI and K_2O, MgO, TiO_2, Rb, Ba, Zr, Nb, and Lu (Supplementary data Fig. S2), combined with the negligible Ce anomalies, argue against a significant influence of alteration on the LILE, HFSE, and REE contents of the samples. The coherent variations in immobile and mobile elements on primitive-mantle-normalized trace-element diagrams also support such a conclusion (Fig. 4). Thus, the geochemical data can be used for ascertaining the origin of these late Paleozoic igneous rocks.

4.1.2. Early Carboniferous calc-alkaline intermediate rocks

The origin of calc-alkaline intermediate rocks has long been one of the most significant and controversial topics in igneous petrology because the geochemical composition of these rocks is comparable to the average composition of continental crust. Various hypotheses for the magma sources of calc-alkaline intermediate rocks have been proposed, including: (i) mafic crustal materials (Jung et al., 2002; Martin et al., 2005), (ii) upper mantle sources (Pichavant and Macdonald, 2007; Grove et al., 2012; Gómez-Tuena et al., 2014; Mitchell and Grove, 2015), and (iii) hybridized sources involving the mixing of mantle- and crust-derived magmas or crustal assimilation of mantle-derived magmas (Cantagrel et al., 1984; Dungan and Davidson, 2004; Reubi and Blundy, 2009).

The possibility that a single mafic crustal material served as the source of the Early Carboniferous calc-alkaline intermediate rocks in the Hailar Basin can be ruled out on the basis of their Mg# values (48–51) and MgO (3.54–3.92 wt.%), Cr (83–104 ppm), and Ni (30–37 ppm) contents, which are higher than those of melts formed by dehydration melting of natural basalts at pressures of 1–4 GPa (Rapp and Watson, 1995; Rapp et al., 1999). A hybridized source for the generation of calc-alkaline intermediate magmas is motivated by the scarcity of intermediate melt inclusion compositions (Reubi and Blundy, 2009), the presence of mafic enclaves (Eichelberger, 1975), and heterogeneous isotopic signatures (Dungan and Davidson, 2004). However, the compositional gap recorded by the melt inclusions are not observed everywhere (Straub, 2003). More importantly, the intermediate rocks we studied lack mafic enclaves and disequilibrium assemblages, and show homogeneous Sr–Nd–Hf isotopic compositions, which are inconsistent with a magma mixing origin. Additionally, these intermediate rocks are characterized by negative Zr and Hf anomalies, an absence of xenocrystic/inherited zircons, and highly depleted isotopic compositions, indicating derivation from an isotopically depleted mantle source without significant crustal contamination. However, compared with primitive-mantle-derived magmas (Mg# > 70, Cr >1000 ppm, and Ni >400–500 ppm; Sharma, 1997; Wilson, 1989), the intermediate rocks we studied have relatively low Mg# values and low Cr and Ni contents, suggesting significant fractional crystallization of ferromagnesian minerals such as olivine and clinopyroxene. Their negligible Eu anomalies and high Sr contents reflect the high H_2O contents (≥4 wt.%) of the initial magmas, which would have inhibited plagioclase fractionation during the early stage of magma evolution (Müntener et al. 2001; Ridolfi et al. 2010).

The Hailar Basin intermediate rocks are enriched in LILEs and depleted in HFSEs, have high La/Nb ratios, low La/Ba ratios, and remarkable Nb–Ta anomalies, making them clearly different from mid-ocean ridge basalt (MORB) and ocean island basalt (OIB) but similar to arc igneous rocks from convergent plate margins. Such characteristics indicate that the mantle source was metasomatized by subduction-related components (Fig. 7a). On a plot of Th/Yb vs Nb/Yb, all our intermediate rock samples plot above the MORB–OIB array (Fig. 7b), providing further support for the involvement of a subduction-related component (Pearce, 2008). Commonly, hydrous melts and aqueous fluids from the subducting slab would serve as metasomatic agents that react with the mantle wedge that overlies the slab–mantle interface in the subduction channel, thus transferring subduction-related components into the mantle source (Zheng, 2019). The relatively constant Nb/Y ratios with increasing Rb/Y ratios and Ba contents define a fluid metasomatism trend (Fig. 8a, b), indicating the mantle sources were modified predominantly by slab-derived aqueous fluids rather than hydrous melts. This inference is further supported by a plot of $(Hf/Sm)_N$

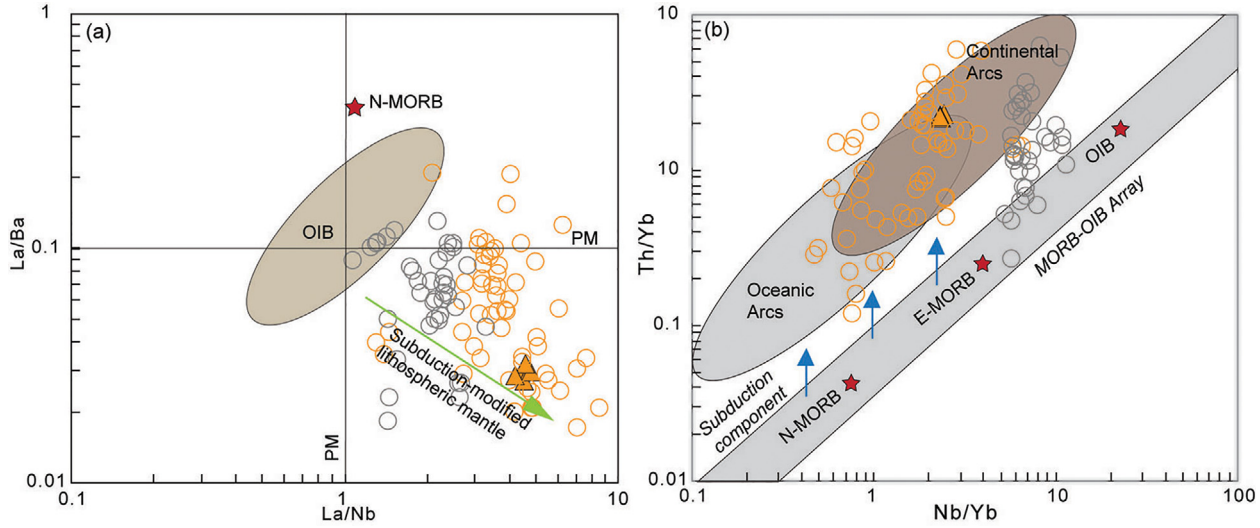

Fig. 7. Plots of (a) La/Ba vs La/Nb (after Saunders et al., 1992) and (b) Th/Yb vs Nb/Yb (after Pearce, 2008) for the Early Carboniferous igneous rocks in the Hailar Basin. Symbols are the same as those in Fig. 4.

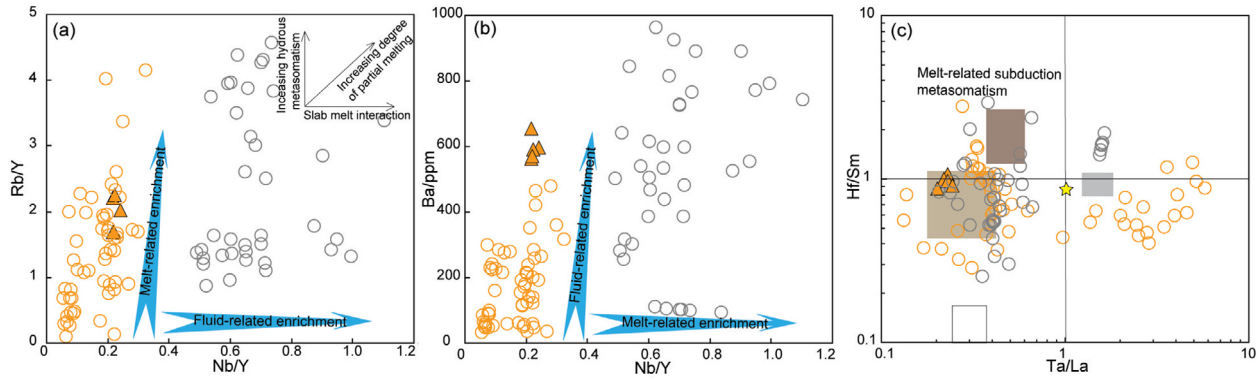

Fig. 8. Plots of (a) Rb/Y vs Nb/Y, (b) Ba vsNb/Y (after Kepezhinskas et al., 1997), and (c) $(Hf/Sm)_N$ vs $(Ta/La)_N$ (after LaFlèche et al., 1998) for the Early Carboniferous igneous rocks in the Hailar Basin. Subscript N indicates primitive mantle normalization (Sun and McDonough 1989). Symbols are the same as those in Fig. 4.

vs $(Ta/La)_N$, as all the data for the intermediate rocks we studied plot in the field of fluid-related subduction metasomatism (Fig. 8c). Additionally, these intermediate rocks have moderate Dy/Yb and Sm/Yb ratios, which plot between the partial melting curves of garnet- and spinel-facies lherzolite (Fig. 9), implying the presence of a garnet + spinel mineral assemblage in the upper mantle source, corresponding to depths of 75–85 km (McKenzie and O'Nions, 1991; Klemme and O'Neill, 2000; Ma et al., 2014). We suggest, therefore, that the intermediate rocks from the Hailar Basin were derived from the partial melting of a depleted mantle wedge metasomatized by slab-derived fluids at depths of 75–85 km, with extensive fractional crystallization of ferromagnesian minerals and insignificant crustal contamination during their magmatic evolution.

4.1.3. Late Carboniferous–Early Permian adakitic rocks

The Late Carboniferous–Early Permian intermediate–acidic rocks have high Sr contents, low Y and HREE contents, and high Sr/Y and $(La/Yb)_N$ ratios, geochemically resembling adakites (Fig. 4c). The term 'adakite' was originally proposed as a genetic term to define a group of intermediate–acidic ($SiO_2 \geq 56$ wt.%) calc-alkaline volcanic rocks and corresponding intrusive rocks derived by partial melting of the basaltic portion of young and hot oceanic crust under eclogite-facies conditions in a subduction environment (Defant and Drummond, 1990; Martin et al., 2005). Although adakites occur in Cenozoic intra-oceanic arcs such as the Aleutian, Izu–Bonin–Mariana, and Solomon–Fiji–Tonga arcs (Yogodzinski et al., 1995; Danyushevsky et al., 2008), intermediate–acidic rocks with similar geochemical features have also been identified in continental arcs, continental collision zones, and intra-continental environments (Kay and Kay, 1991; Gutscher et al., 2000; Beate et al., 2001; Chung et al., 2003; Gao et al., 2004; Yin et al., 2017; Ji et al., 2021), thus leading to controversy over the origin of adakitic rocks. As a result, several models have been proposed, including crustal assimilation and fractional crystallization (AFC) of parental mafic magmas (Castillo et al., 1999; Macpherson et al., 2006), magma mixing of felsic and mafic magmas (Guo et al., 2007; Streck et al., 2007), and partial melting of thickened or foundered lower crust (Kay and Kay, 1991; Xu et al., 2002; Gao et al., 2004; Wang et al., 2006).

Adakitic rocks derived by AFC processes in mafic magmas (e.g., high- or low-pressure fractional crystallization involving garnet or amphibole with high partition coefficients for Y and HREEs) are spatially and temporally associated with voluminous mafic rocks that exhibit systematic geochemical and isotopic correlations (Castillo et al., 1999; Macpherson et al., 2006). However, the geological data for our study area indicate that exposed areas of contemporaneous mantle-derived mafic rocks are quite limited

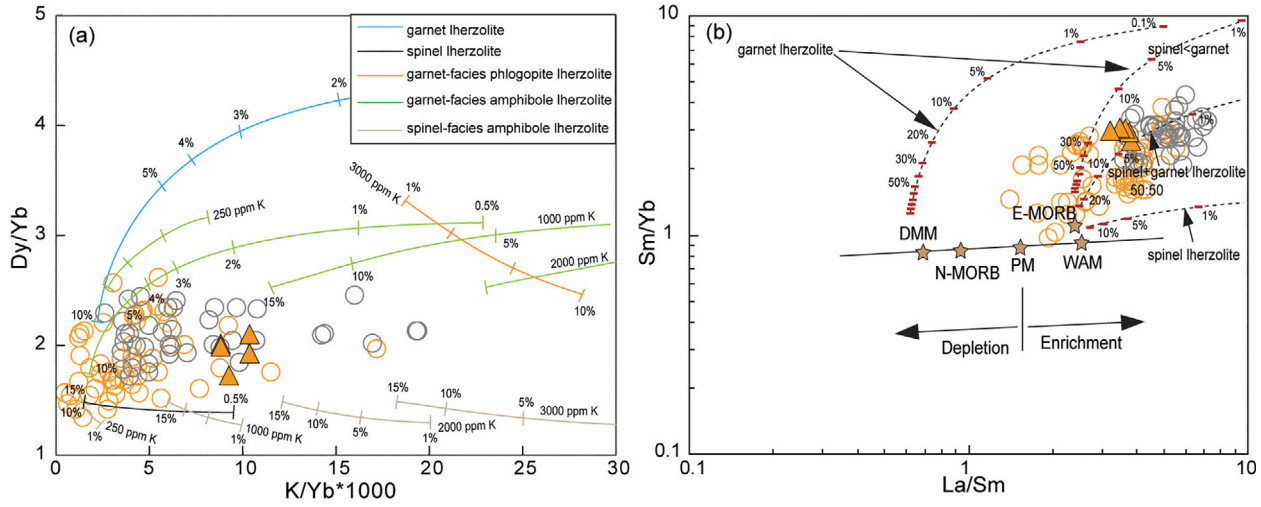

Fig. 9. Plots of (a) Dy/Yb vs K/Yb × 1000 (after Ma et al., 2014) and (B) Sm/Yb vs La/Sm (after Bi et al., 2017) for the Early Carboniferous igneous rocks in the Hailar Basin. Symbols are the same as those in Fig. 4.

(Meng et al., 2013), and these small amounts of mafic magma could not have produced such large volumes of Late Carboniferous–Early Permian adakitic rocks by AFC processes. Moreover, high-pressure fractional crystallization of garnet would have raised the Sr/Y and Dy/Yb ratios in the residual melts, and low-pressure fractional crystallization of amphibole would have lowered the Dy/Yb ratio, as amphibole has D(Dy)/D(Yb) >1 (Rollinson, 1993). However, the lack of strong correlations between SiO_2 contents and Sr/Y and Dy/Yb ratios for these adakitic rocks preclude fractionation of garnet or amphibole (Fig. 10a and b). Furthermore, our adakitic rock samples display a partial melting trend rather than a fractional crystallization trend on the La/Yb vs La diagram (Fig. 10c). Combining these characteristics with the simple mineralogy and uniform Sr–Nd–Hf isotope compositions of our samples, and taking into account the absence of mafic enclaves and mixing textures as well as the correlation between initial Sr isotopic compositions and SiO_2 contents, we suggest that the adakitic signatures of the Late Carboniferous–Early Permian adakitic rocks in our study area were probably derived directly from the magma source rather than from AFC or magma mixing processes.

The potential crustal sources of adakitic rocks include subducting oceanic crust and normal/thickened/foundered lower continental crust (Defant and Drummond, 1990; Kay and Kay, 1991; Chung et al., 2003; Gao et al., 2004). Adakitic rocks derived from partial melting of basaltic oceanic crust commonly exhibit high sodium contents ($K_2O/Na_2O \approx 0.42$) and low Rb/Sr (< 0.05) and Th/La (< 0.3) ratios with oceanic crustal isotopic compositions (Martin et al., 2005; Wang et al., 2008; Huang et al., 2013). However, the Late Carboniferous–Early Permian adakitic rocks in the Hailar Basin that belong to the high-K calc-alkaline series show high K_2O/Na_2O (0.5–0.9), Rb/Sr (0.037–0.32), and Th/La (0.15–0.57) ratios, which are clearly different from oceanic crust-derived adakitic rocks. In addition, on a K–Na–Ca ternary diagram, the Late Carboniferous–Early Permian adakitic rocks plot outside the field of oceanic-crust-derived adakitic rocks, but within the field of continental adakitic rocks (Fig. 11), which indicates they are continental adakitic rocks. Moreover, the adakitic rocks of the Hailar Basin have much lower $\varepsilon_{Nd}(t)$ values (3.72–6.48) than MORB-like gabbros from the Hegenshan ophiolite that are considered to represent the remnants of Nenjiang oceanic crust (Fig. 6a). Although the involvement of subducting sediments in oceanic slab melts would account well for the low $\varepsilon_{Nd}(t)$ values and high K_2O/Na_2O, Rb/Sr, and Th/La ratios of the Hailar Basin adakitic rocks, their low $^{87}Sr/^{86}Sr$ ratios plot some distance from the model mixing curve for the whole-rock Sr–Nd isotopic compositions of Hegenshan ophiolite and global subducting sediments (GLOSS) (Fig. 6b), and this rules out an origin linked to the partial melting of basaltic oceanic crust with some addition of subducting-sediment-derived material.

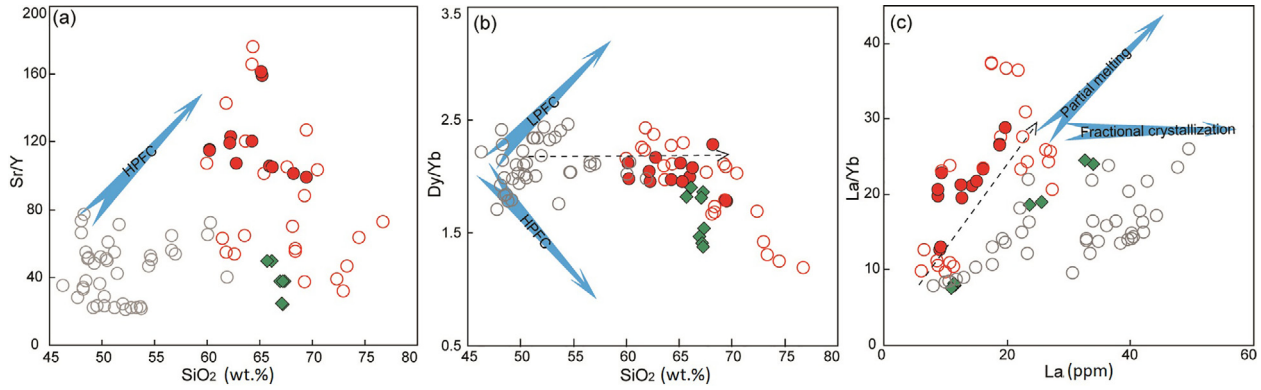

Fig. 10. Plots of (a) Sr/Y vs SiO_2, (b) Dy/Yb vs SiO_2, and (c) La/Yb vs La (after Wang et al., 2008) for the Late Carboniferous–Early Permian adakitic rocks in the Hailar Basin. Symbols are the same as those in Fig. 4.

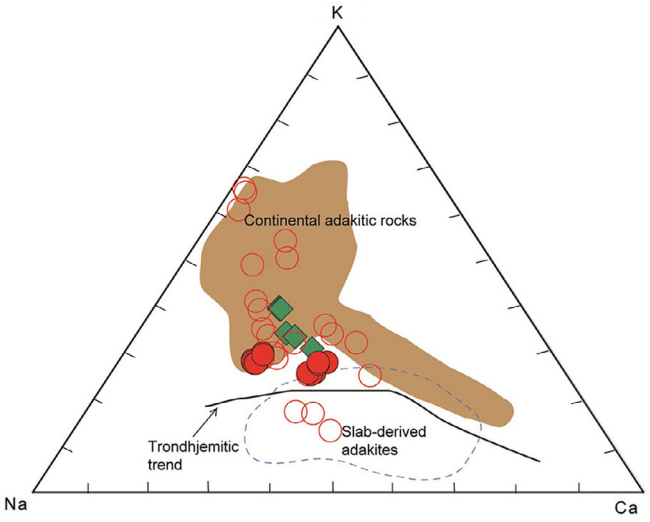

Fig. 11. K–Na–Ca diagram (after Oh et al., 2016) for the the Late Carboniferous–Early Permian adakitic rocks in the Hailar Basin. Symbols are the same as those in Fig. 4.

Continental adakitic rocks are commonly inferred to be the products of partial melting of thickened/foundered lower continental crust at depths >40–50 km (Xu et al., 2002; Chung et al., 2003; Gao et al., 2004). However, recent melting experiments and modeling have shown that although a pressure of $\geq$ 15 kbar may be required to produce oceanic-crust-derived adakitic rocks from MORB, high-pressure processes are not necessary for the formation of continental adakitic rocks (Ma et al., 2015). In fact, continental adakitic rocks can be generated at pressures less than 12.5 kbar, and their high Sr/Y ratios probably reflect a Sr/Y rich source, such as normal lower continental crust, regardless of the melting depth (Moyen, 2009). It is therefore critical to ascertain the effects of source inheritance and high-pressure melting when considering the origin of the Late Carboniferous–Early Permian continental adakitic rocks of the Hailar Basin. The high-K calc-alkaline adakitic rocks of the Hailar Basin have Y, Yb, Sr/Y, and Gd/Yb values that are distinct from those of the calc-alkaline adakitic rocks, indicating different pressures of melting (Qian and Hermann et al., 2013). Moreover, on a $(Sr/Y)_N$ vs. Y_N diagram (Fig. 12a), the calc-alkaline adakitic rocks plot within the field for melts produced by melting of lower continental crust at 13.5–15 kbar and 900–1000 °C (corresponding to depths of 45–50 km), indicating deep melting of a mafic source (i.e., thickened/foundered lower continental crust). Nevertheless, the high-K calc-alkaline adakitic rocks plot within the field for melts produced from lower continental crust at 10–12.5 kbar and 800 °C (corresponding to depths of 30–40 km), reflecting the melting of a mafic source at relatively shallow depths (i.e., within normal lower continental crust). In addition, continental adakitic rocks derived from thickened/foundered lower continental crust have systematically higher $(Sm/Yb)_{SN}$ and lower Yb_{SN} values than continental adakitic rocks derived from normal lower continental crust (Ma et al., 2015). On a source-normalized diagram, the calc-alkaline adakitic rocks of the Hailar Basin show high values of $(Sm/Yb)_{SN}$ and low values of Yb_{SN}, similar to adakitic rocks from collisional orogens and modeled melts in equilibrium with a garnet-rich residue (Fig. 12b). In contrast, the high-K calc-alkaline adakitic rocks have lower values of $(Sm/Yb)_{SN}$ and higher values of Yb_{SN}, similar to adakitic rocks from regions that lack evidence for a thickened lower continental crust and modeled melts in equilibrium with a residue that lacks garnet. Therefore, the calc-alkaline adakitic rocks and the high-K calc-alkaline adakitic rocks probably formed by partial melting of thickened/foundered lower continental crust and normal lower continental crust, respectively. Notably, the calc-alkaline adakitic rocks have higher Cr, Ni, and MgO concentrations and Mg# (47–55) values than thickened lower continental crust-derived adakitic rocks and experimental melts derived from natural hydrous basalts at 1–4 GPa (Rapp et al., 1999). This indicates that the pristine adakitic melts were derived from foundered and eclogitized lower continental crust, with these melts subsequently interacting with mantle peridotites during ascent (Xu et al., 2002; Gao et al., 2004; Wang et al., 2006). To quantitatively evaluate melt–mantle interactions, we performed simple two end-member mixing modeling for the calc-alkaline adakitic rocks using major-element concentrations. The modeling results suggest the involvement of ~16% mantle material in the calc-alkaline adakitic rocks (Fig. 12c).

4.2. Tectonic settings of magma generation

The late Paleozoic tectonic evolution of the XEB was controlled mainly by the closure of the Nenjiang Ocean (a branch of the Paleo-Asian Ocean) and associated subduction processes. Subduction of the Nenjiang oceanic slab beneath the XEB is generally considered to have commenced during the Late Cambrian–Middle Ordovician

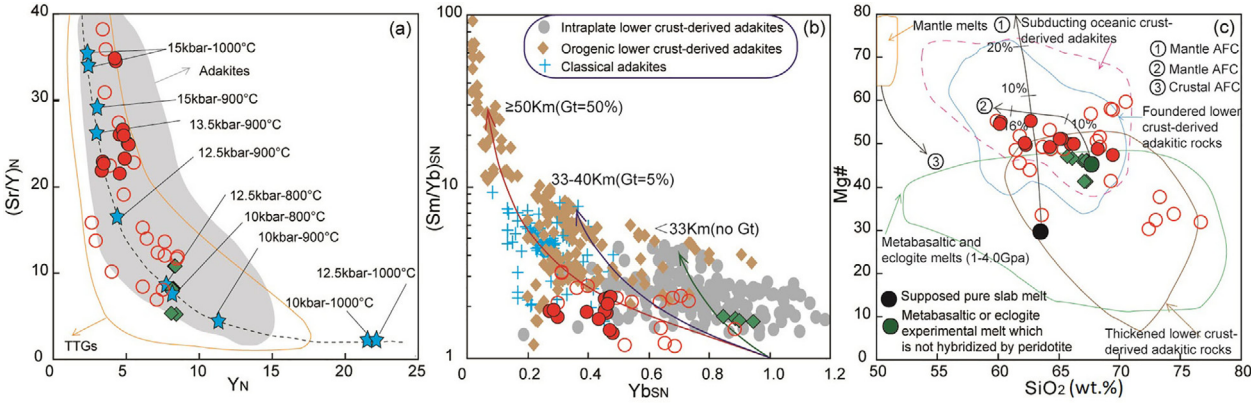

Fig. 12. Plots of (a) $(Sr/Y)_N$ vs Y_N (after Qian and Hermann, 2013), (b) $(Sm/Yb)_{SN}$ vs Yb_{SN} (after Ma et al., 2015), and (c) Mg# vs SiO_2 (after Wang et al., 2006) for the Late Carboniferous–Early Permian adakitic rocks in the Hailar Basin. Data for the intraplate lower crust-derived adakites, orogenic lower crust-derived adakites, and classical adakites are from Ma et al. (2015) and references therein. Subscript N means chondrite normalization (Sun and McDonough 1989). Subscript SN denotes source normalization, where the compositions of the assumed sources are MORB with Yb = 3 ppm and Sm/Yb = 1.08 for classical adakites and those from the Central Andes, and the mafic lower continental crust with Yb = 1.5 ppm and Sm/Yb = 1.87 for continental adakitic rocks. Symbols are the same as those in Fig. 4.

or earlier, as recorded by the Duobaoshan–Moguqi–Baiyanbaoli dao–Hadaaobao arcs (508–462 Ma) and the Xinglin–Aershan back-arc basins (480–463 Ma) along the eastern XEB (Feng et al., 2018a; Liu et al., 2021). However, timing of closure of the Nenjiang Ocean and collision of the XEB and the SB remains controversial, with diverse suggestions including Early–Middle Devonian (Tang, 1990; Su, 1996; Zhao et al., 2013; Xu et al., 2015), late Early Carboniferous–early Late Carboniferous (Zhao et al., 2010; Li et al., 2014; Liu et al., 2017; Ji et al., 2018; Zhang et al., 2018), pre-Permian (Sun et al., 2000; Zhang et al., 2021), or late Permian–Early Triassic (Miao et al., 2008; Yu et al., 2017; Yang et al., 2019).

Based on the unconformity between the Upper Devonian conglomerates and sandstones and the underlying ophiolitic mélanges in the Sunid Zuoqi, and their different deformation patterns, Xu et al. (2015) proposed that the Nenjiang Ocean was closed during the Early–Middle Devonian to form the Hegenshan–Heihe Suture. However, this inference is inconsistent with the following stratigraphic and magmatic evidence. Firstly, the unconformity is not observed in other areas of the XEB, and the XEB is largely covered by continuous Late Devonian–Early Carboniferous marine strata, which indicates that the ocean basin was still in existence during the Late Devonian–Early Carboniferous. In other words, the unconformity probably records only a local transgressive event (Li, 2006). Secondly, there is a lack of Devonian S-type granites in the XEB, which indicates that the XEB–SB collision did not occur during the Devonian. Finally, the Early Carboniferous calc-alkaline intermediate rocks we studied are characterized by enrichments in LREEs and LILEs (e.g., Rb, Ba, and K) and depletions in HREEs and HFSEs (e.g., Nb, Ta, and Ti), and they originated from the partial melting of a depleted mantle wedge that was modified by slab-derived fluids. These characteristics are analogous to those of igneous rocks that form along active continental margins, indicating an oceanic subduction setting rather than a *syn*-collisional or post-collisional setting. This hypothesis is further supported by tectonic discrimination diagrams, as data for the Late Devonian–Early Carboniferous intermediate–basic rocks from both sides of the Hegenshan–Heihe Suture plot in typical volcanic arc fields (Fig. 13). Thus, the existence of a Late Devonian–Early Carboniferous double-sided subduction system and the presence of marine strata preclude a Devonian timing for closure of the Nenjiang Ocean.

Notably, some workers have even argued that subduction of the Nenjiang oceanic slab continued until the Late Permian, and that amalgamation of the XEB and SB occurred during the Late Permian–Early Triassic (Miao et al., 2008; Yu et al., 2017; Yang et al., 2019). However, the latest paleomagnetic studies have shown insignificant paleo-latitudinal differences between the XEB (34.0°N ± 3.8°N) and the SB (33.2°N ± 5.4°N) at the Carboniferous–Permian boundary (Zhang et al., 2021), indicating that amalgamation of the XEB and SB occurred before the latest Carboniferous. We propose here that the Nenjiang Ocean was probably closed by the latest Early Carboniferous, based on the following three lines of geological evidence: (i) Relics of the Nenjiang oceanic crust are well preserved in the Erenhot and Hegenshan ophiolite mélanges. Zircon U–Pb dating has shown that gabbros and plagiogranites from the Erenhot ophiolite mélange were formed at ca. 354–345 Ma, and that an undeformed and unmetamorphosed dioritic porphyry dike was intruded into the Erenhot ophiolite at ca. 314 Ma (Zhang et al., 2015), which means that the Erenhot ophiolite mélange was emplaced between 345 Ma and 314 Ma. In addition, the Hegenshan ophiolite mélanges in the Chongenshan–Hegenshan–Wunisihei area, including ca. 359–341 Ma mafic rocks and ca. 333 Ma plagiogranites, are unconformably overlain by the upper Carboniferous Gegenaobao Formation and the middle Permian Zhesi Formation (Jian et al., 2012; Zhou et al., 2015; Huang et al., 2016). The volcanic rocks in the Gegenaobao Formation have eruptive ages of ca. 323–300 Ma, which provide an upper time limit for the emplacement of the Hegenshan ophiolite mélanges (Jian et al., 2012; Huang et al., 2016). These lithostratigraphic relationships indicate that subduction of the Nenjiang oceanic slab had ceased by the latest Early Carboniferous. (ii) A transition in the sedimentary facies of the XEB from Early Carboniferous marine strata (i.e., the Hongshuiquan, Moergenhe, Xieertala, and Gaojiaoshan formations that consist mainly of limestones, shales, sandstones, cherts, tuffs, and keratophyres) to Late Carboniferous terrestrial strata (i.e., the Yigenhe and Baoligemiao formations that consist mainly of sandstones, conglomerate, mudstones, and volcanic rocks) indicates the occurrence of a major tectonic event during the latest Early Carboniferous, probably corresponding to the closure of the Nenjiang Ocean between the XEB and the SB (IMBGMR, 1991; Li et al., 2014; Zhao et al., 2010). (iii) The Late Devonian to Early Carboniferous

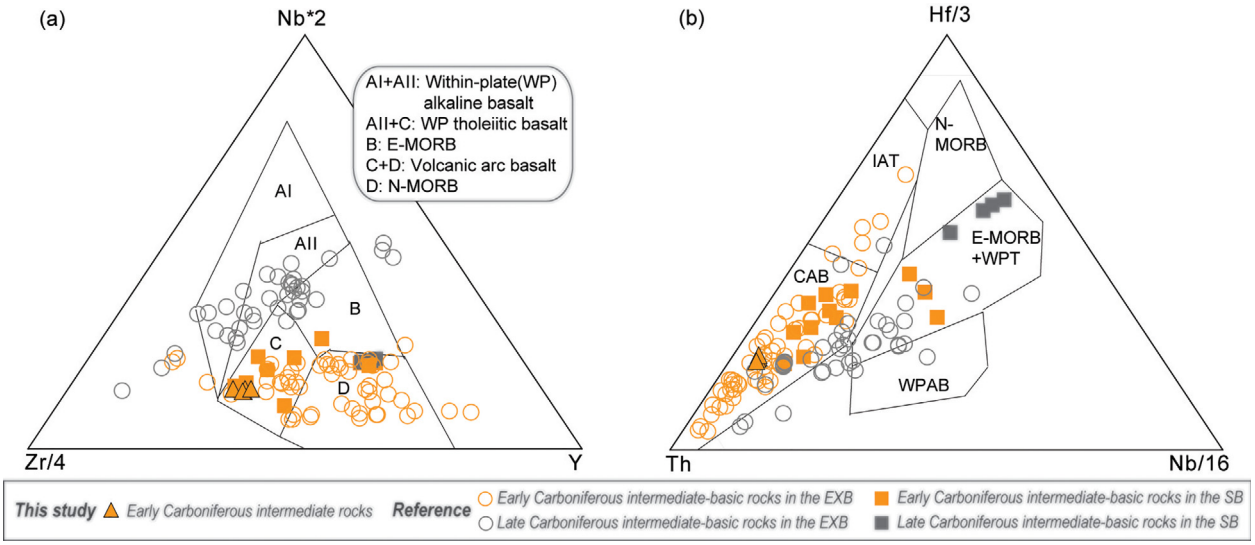

Fig. 13. Tectonic discrimination diagrams for the Carboniferous intermediate–basic rocks in the Xing'an–Erguna Block and the Songliao Basin. (a) 2Nb–Zr/4–Y diagram (after Meschede, 1986). (b) Hf/3–Th–Nb/16 diagram (after Wood 1980). Data for the Early Carboniferous intermediate–basic rocks in the Songliao Basin are from Ma et al. (2020a) and Wang et al. (2013). Data for the Late Carboniferous intermediate–basic rocks in the Songliao Basin are from Ma et al. (2020b).

mafic rocks in the XEB have characteristics similar to those of arc igneous rocks, whereas the Late Carboniferous mafic rocks have geochemical features indicating a within-plate setting (Fig. 13). Such a distinct change in the nature and composition of the magma possibly implies a rapid tectonic switch from oceanic subduction to post-collisional extension during the latest Early Carboniferous. Furthermore, unlike the widespread Early Carboniferous subduction-related I-type granitic magmatism in the XEB, the Late Carboniferous–Early Permian magmatic activity was characterized by A_2-type granitoids, high-Mg adakitic rocks, and bimodal magmatic suites (Wu et al., 2002, 2011; Ji et al., 2018; Zhang et al., 2018), all of which indicate post-collisional extension during the late Carboniferous–Early Permian.

In summary, taking into consideration the latest Early Carboniferous closure time of the Nenjiang Ocean, we suggest that the Late Devonian–Early Carboniferous magmatic rocks along the Hegenshan–Heihe Suture were formed in an oceanic subduction setting, while the Late Carboniferous–Early Permian magmatic rocks were generated in a post-collisional extensional setting.

4.3. Implications for post-collisional lithospheric dripping in soft collision zones

The Hegenshan–Heihe Suture records a series of evolutionary processes, including Early Carboniferous double-sided subduction of the Nenjiang oceanic crust (359–331 Ma), latest Early Carboniferous soft collision between the XEB and the SB (330–323 Ma), and Late Carboniferous–Early Permian post-collisional extension (323–273 Ma), consequently providing an excellent opportunity to ascertain the post-collisional geodynamic processes that operated in a soft collision zone driven by divergent double-sided subduction.

Post-collisional tectonomagmatic events in a soft collision zone are often attributed to slab break-off that is almost inevitable several to ten million years after the initial continental collision (Davies and von Blanckenburg, 1995; Soesoo et al., 1997; Gerya et al., 2004; Rosenbaum et al., 2008; Zhu et al., 2015; Zhu et al., 2016). A direct response to slab break-off is the upwelling of hot asthenospheric mantle that could trigger rapid topographic uplift and partial melting of magma source regions, thus producing magmas that could potentially deviate from the geochemistry of typical subduction-related magmas (including within-plate basaltic magmatism, bimodal magmatism, and A-type granitic magmatism) (Soesoo et al., 1997; Gerya et al., 2004; Prelević et al., 2015; Freeburn et al., 2017). In the case of the Hegenshan–Heihe Suture, slab break-off can explain the rapid change in the nature and composition of the Carboniferous magmas. Furthermore, latest Early Carboniferous–Late Carboniferous slab break-off involving concomitant topographic uplift is also consistent with a lack of sedimentation along the Hegenshan–Heihe Suture during the Serpukhovian, Bashkirian, and Moscovian stages. Notably, the slab break-off model does not explain the temporal and spatial distri-

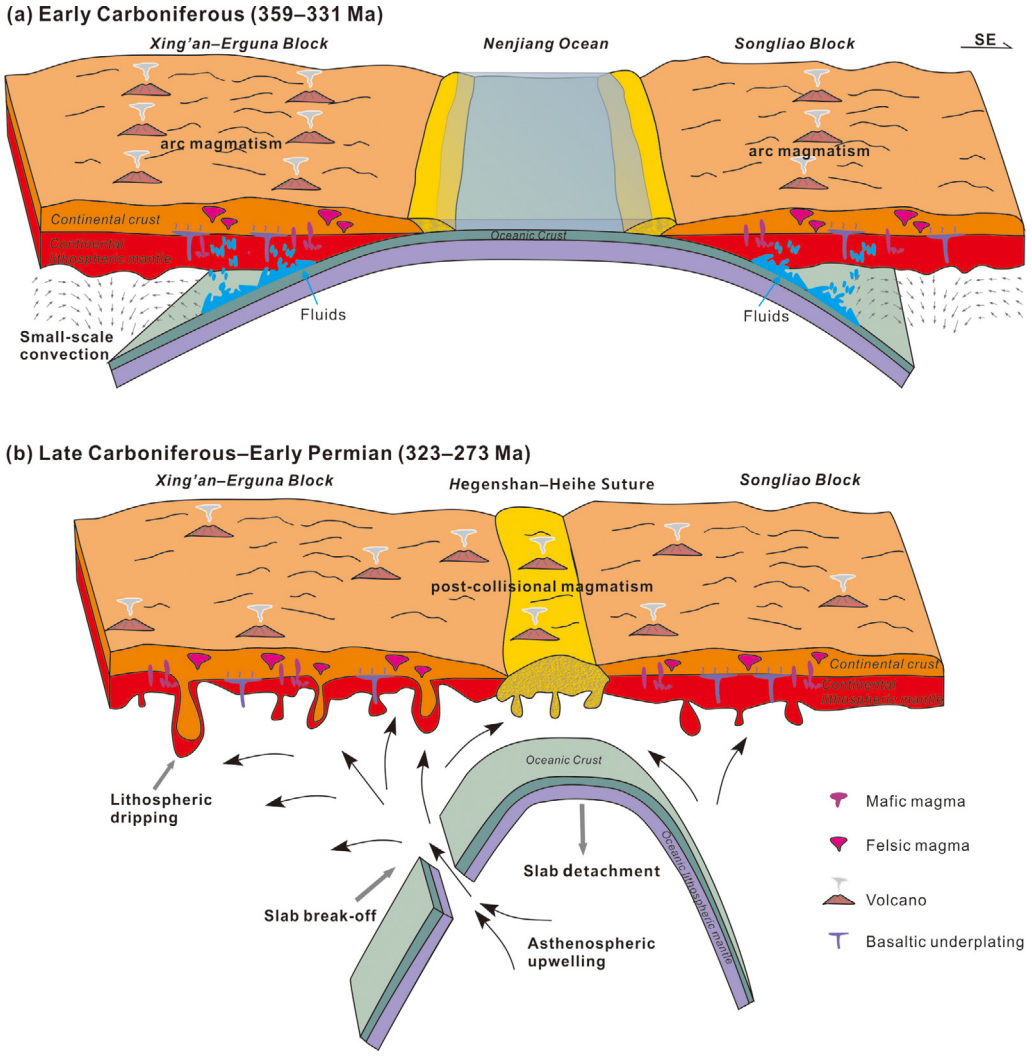

Fig. 14. Schematic cartoons showing geodynamic evolution of the Hegenshan–Heihe Suture during the Early Carboniferous–Early Permian.

bution of post-collisional magmatic activity in the XEB because propagation of slab break-off would be expected to produce a short-lived linear zone of magmatism near the suture (Davies and von Blanckenburg, 1995; Macera et al., 2008), whereas the Late Carboniferous–Early Permian post-collisional magmatic activity in the XEB has a long history and occurred hundreds of kilometers from the suture, without a clear time-space relationship. Thus, it is unlikely that the slab break-off process by itself can account for all the observations of the post-collisional magmatism. Additional mechanisms are required to explain the diverse nature of the post-collisional tectonomagmatic events in the XEB.

Metasomatism induced by fluids from the subducted Nenjiang oceanic slab occurred in the mantle wedge beneath the XEB, as indicated by the widespread Late Devonian–Early Carboniferous arc igneous rocks (Wu et al., 2011; Liu et al., 2017; Zhang et al., 2018; Li et al., 2020). Such a process can potentially transport large quantities of water to the lithospheric mantle and modify the water content of the mantle by the precipitation of new volatile-rich minerals (e.g., amphibole and phlogopite) and incorporation of hydrogen into crystal defects of nominally anhydrous minerals (e.g., olivine and pyroxene) (O'Reilly and Griffin, 2013; Bell and Rossman, 1992; Peslier et al., 2012; Demouchy et al., 2015). Deformation experiments and thermomechanical numerical models have demonstrated that water has a significant weakening effect on the viscosity of the lithospheric mantle as only a small amount of H_2O can remarkably decrease the stress of dislocation and diffusion creep of olivine (Wang, 2010; Liao et al., 2017). Thus, pre-collision subduction of the Nenjiang oceanic slab would have reduced the contrast in viscosity between the lithospheric mantle and the surrounding asthenospheric mantle, led to hydration-induced rheological weakening of lithosphere, and so to small-scale convection at the lithosphere–asthenosphere boundary in the XEB (Hernlund et al., 2008; Kaislaniemi et al., 2014) (Fig. 14a). Asthenospheric upwelling induced by break-off of the subducted Nenjiang oceanic slab after the collision of the XEB and SB would have further increased vigor of the convection and triggered Rayleigh–Taylor convective instability of the hydration-weakened lithospheric root (Houseman and Molnar, 1997; Gorczyk et al., 2012), eventually causing the root to drip into the underlying asthenosphere (Ducea, 2011; Kaislaniemi et al., 2014; Liao et al., 2017) (Fig. 14b). In contrast to large-scale lithospheric delamination that predicts the presence of extensive mafic and high-Mg adakitic magmatism as a result of wholesale peeling of a coherent block of the lithosphere away from the overlying crust (Bird, 1979; Kay and Kay, 1993; Ducea and Saleeby, 1998), lithospheric dripping can lead to volumetrically variable mafic and high-Mg adakitic magmatism, depending on the sizes of the drips (Drew et al., 2009; Ducea, 2011). The absence of large-scale crustal shortening and mountain building, as well as the occurrence of the minor post-collisional mafic igneous rocks and high-Mg adakitic rocks in the XEB indicate that the post-collisional tectonomagmatic events were primarily controlled by lithospheric dripping rather than large-scale lithospheric delamination, and the size of the drips is small. Considering that the Late Carboniferous–Early Permian post-collisional magmatism in the XEB was a protracted process, and was scattered in time and space, we conclude that repeated and localized lithospheric dripping took place after the soft collision of the XEB and SB, leading to the removal of the moderately thickened orogenic lithosphere.

5. Conclusions

(i) Early Carboniferous arc-like igneous rocks and Late Carboniferous–Early Permian adakitic rocks occur in the Hailar Basin of the XEB.

(ii) The Early Carboniferous arc-like igneous rocks were generated by partial melting of a depleted mantle wedge that had been metasomatized by fluids derived from a subducted slab. The late Carboniferous–Early Permian adakitic rocks can be subdivided into calc-alkaline adakitic rocks and high-K calc-alkaline adakitic rocks. The former were formed by partial melting of foundered lower continental crust, and the latter by partial melting of normal lower continental crust.

(iii) The transition from double-sided subduction of the Nenjiang oceanic plate to the soft collision of the XEB and SB occurred during the latest Early Carboniferous.

(iv) Repeated and localized lithospheric dripping is proposed to explain the post-collisional magmatism in soft collision zones.

Declaration of Competing Interest

The authors declare that they have no known competing financial interests or personal relationships that could have appeared to influence the work reported in this paper.

Acknowledgments

This work was financially supported by the National Natural Science Foundation of China (Grants Nos. 41888101, 42102046, and 92062216).

Appendix A. Supplementary data

Supplementary data to this article can be found online at https://doi.org/10.1016/j.gsf.2022.101462.

References

Beate, B., Monzier, M., Spikings, R., Cotten, J., Silva, J., Bourdon, E., Eissen, J.P., 2001. MioPliocene adakite generation related to flat subduction in southern Ecuador: the Quimsacocha volcanic center. Earth Planet. Sci. Lett. 192, 561–570.

Bell, D.R., Rossman, G.R., 1992. Water in Earth's mantle: the role of nominally anhydrous minerals. Science 255, 1391–1397.

Bi, J.H., Ge, W.C., Yang, H., Wang, Z.H., Tian, D.X., Liu, X.W., Xu, W.L., Xing, D.H., 2017. Geochemistry of MORB and OIB in the Yuejinshan Complex, NE China: implications for petrogenesis and tectonic setting. J. Asian Earth Sci. 145, 475–493.

Bird, P., 1979. Continental Delamination and the Colorado Plateau. J. Geophys. Res. 84, 7561–7571.

Cantagrel, J.M., Didier, J., Gourgaud, A., 1984. Magma mixing: origin of intermediate rocks and "enclaves" from volcanism to plutonism. Phys. Earth Planet. Inter. 35, 63–76.

Castillo, P.R., Janney, P.E., Solidum, R., 1999. Petrology and geochemistry of Camiguin Island, southern Philippines: insights into the source of adakite and other lavas in a complex arc tectonic setting. Contrib. Mineral. Petrol. 134, 33–51.

Chung, S.L., Liu, D.Y., Ji, J.Q., Chu, M.F., Lee, H.Y., Wen, D.J., Lo, C.H., Lee, T.Y., Qian, Q., Zhang, Q., 2003. Adakites from continental collision zones: melting of thickened lower crust beneath southern Tibet. Geology 31, 1021–1024.

Chung, S.L., Chu, M.F., Zhang, Y.Q., Xie, Y.W., Lo, C.H., Lee, T.Y., Lan, C.Y., Li, X.H., Zhang, Q., Wang, Y.Z., 2005. Tibetan tectonic evolution inferred from spatial and temporal variations in post-collisional magmatism. Earth Sci. Rev. 68, 173–196.

Compagnoni, R., 2003. HP metamorphic belt of the western Alps. Episodes 26, 200–204.

Danyushevsky, L.V., Falloon, T.J., Crawford, A.J., Tetroeva, S.A., Leslie, R.L., Verbeeten, A., 2008. High-Mg adakites from Kadavu Island Group, Fiji, southwest Pacific: evidence for the mantle origin of adakite parental melts. Geology 36, 499–502.

Davies, J.H., von Blanckenburg, F., 1995. Slab breakoff: a model of lithosphere detachment and its test in the magmatism and deformation of collisional orogens. Earth Planet. Sci. Lett. 129, 85–102.

Defant, M.J., Drummond, M.S., 1990. Derivation of some modern arc magma by melting of young subducted lithosphere. Nature 347, 662–665.

Demouchy, S., Ishikawa, A., Tommasi, A., Alard, O., Keshav, S., 2015. Characterization of hydration in the mantle lithosphere: peridotite xenoliths from the Ontong Java Plateau as an example. Lithos 212–215, 189–201.

Dong, Y., Ge, W.C., Zhao, G.C., Yang, H., Liu, X.W., Zhang, Y.L., 2016. Petrogenesis and tectonic setting of the Late Paleozoic Xing'an complex in the northern Great Xing'an Range, NE China: constraints from geochronology, geochemistry and zircon Hf isotopes. J. Asian Earth Sci. 115, 228–246.
Dong, Y., He, Y., Ge, W.C., Yang, H., Ji, Z., Bi, J.H., Wang, Z.H., Yu, Q., Zhao, D., 2020. Important role of magma mixing in generating the late Carboniferous Tayuan Complex during subduction of the Paleo-Asian oceanic plate beneath the Xing'an–Erguna Massif, NE China: Evidence from petrology,geochemistry, and zircon U–Pb–Hf isotopes. Lithos 370–371, 105617.
Drew, S.T., Ducea, M.N., Schoenbohm, L.M., 2009. Mafic volcanism on the Puna Plateau, NW Argentina: Implications for lithospheric composition and evolution with an emphasis on lithospheric foundering. Lithosphere 1, 305–318.
Ducea, M.N., 2011. Fingerprinting orogenic delamination. Geology 39, 191–192.
Ducea, M.N., Saleeby, J.B., 1998. A case for delamination of the deep batholithic crust beneath the Sierra Nevada. California. Int. Geol. Rev. 40, 78–93.
Dungan, M.A., Davidson, J., 2004. Partial assimilative recycling of the mafic plutonic roots of arc volcanoes: an example from the Chilean Andes. Geology 32, 773–776.
Eichelberger, J.C., 1975. Origin of andesite and dacite; evidence of mixing at Glass Mountain in California and at other Circum-Pacific volcanoes. Geol. Soc. Am. Bull. 86, 1381–1391.
Eizenhöfer, P.R., Zhao, G., Sun, M., Zhang, J., Han, Y., Hou, W., 2015. Geochronological and Hf isotopic variability of detrital zircons in Paleozoic strata across the accretionary collision zone between the North China craton and Mongolian arcs and tectonic implications. Geol. Soc. Am. Bull. 127, 1422–1436.
Eizenhöfer, P.R., Zhao, G.C., 2018. Solonker Suture in East Asia and its bearing on the final closure of the eastern segment of the Palaeo-Asian Ocean. Earth Sci. Rev. 186, 153–172.
Feng, Z.Q., Liu, Y.J., Liu, B.Q., Wen, Q.B., Li, W.M., Liu, Q., 2016. Timing and nature of the Xinlin–Xiguitu Ocean: constraints from ophiolitic gabbros in the northern Great Xing'an range, eastern Central Asian Orogenic Belt. Int. J. Earth Sci. 105, 491–505.
Feng, Z.Q., Liu, Y.J., Wen, Q.B., Han, G.Q., Li, W.M., Zhang, L., 2014. Daxinanling northern section of the tower becomes the source region ~330Ma gabbro–granite petrogenesis and tectonic significance of. Acta Petrol. Sin. 30. in Chinese with English abstract.
Feng, Z.Q., Jia, J., Liu, Y.J., Wen, Q.B., Li, W.M., Liu, B., Xing, D.Q., Zhang, L., 2015. Geochronology and geochemistry of the Carboniferous magmatism in the northern Great Xing'an Range, NE China: Constraints on the timing of amalgamation of Xing'an and Songnen blocks. J. Asian Earth Sci. 113, 411–426.
Feng, Z.Q., Liu, Y.J., Jin, W., Li, W.M., Wen, Q.B., 2017. Is there the Paleoproterozoic komatiite related to mantle plume in the Jifeng area, Northern Great Xing'an Range, NE China? Int. J. Earth Sci. 106, 2225–2231.
Feng, Z.Q., Liu, Y.J., Wu, P., Jin, W., Li, W.M., Wen, Q.B., Zhao, Y.L., Zhou, J.P., 2018a. Silurian magmatism on the eastern margin of the Erguna block, NE China: evolution of the northern Great Xing'an range. Gondwana Res. 61, 46–62.
Feng, Z.Q., Li, W.M., Liu, Y.J., Jin, W., Wen, Q.B., Liu, B.Q., Zhou, J.P., Zhang, T.A., Li, X. Y., 2018b. Early Carboniferous tectonic evolution of the northern Heihe–Nenjiang–Hegenshan suture zone, NE China: Constraints from the mylonitized Nenjiang rhyolites and the Moguqi gabbros. Geol. J. 53, 1005–1021.
Freeburn, R., Bouilhol, P., Maunder, B., Magni, V., Van Hunen, J., 2017. Numerical models of the magmatic processes induced by slab breakoff. Earth Planet. Sci. Lett. 478, 203–213.
Frisch, W., Meschede, M., Blakey, R., 2011. Plate tectonics: continental drift and mountain building. Springer-Verlag, Berlin Heidelberg, pp. 149–158.
Gao, S., Rudnick, R.L., Yuan, H.L., Liu, X.M., Liu, Y.S., Xu, W.L., Ling, W.L., Ayers, J., Wang, X.C., Wang, Q.H., 2004. Recycling lower continental crust in the North China craton. Nature 432, 892–897.
Ge, W.C., Chen, J.S., Yang, H., Zhao, G.C., Zhang, Y.L., Tian, D.X., 2015. Tectonicimplications of new zircon U-Pb ages for the Xinghuadukou complex, Erguna massif,northern Great Xing'an range, NE China. J. Asian Earth Sci. 106, 169–185.
Ge, W.C., Wu, F.Y., Zhou, C.Y., Rahman A.A.A., Rahman, 2005. Emplacement age of the Tahe granite and its constraints on the tectonic nature of the Ergun block in the northern part of the Da Hinggan Range. Chin. Sci. Bull. 50, 2097–2105.
Gerya, T.V., Yuen, D.A., Maresch, W.V., 2004. Thermomechanical modelling of slab detachment. Earth Planet. Sci. Lett. 226, 101–116.
Gómez-Tuena, A., Straub, S.M., Zellmer, G.F., 2014. An introduction to orogenic andesites and crustal growth. Geol. Soc. Spec. Publ. 385, 1–13.
Gorczyk, W., Hobbs, B., Gerya, T., 2012. Initiation of Rayleigh-Taylor instabilities in intracratonic settings. Tectonophysics 514–517, 146–155.
Gou, J., Sun, D.Y., Yang, D.G., Tang, Z.Y., Mao, A.Q., 2019. Late Palaeozoic igneous rocks of the Great Xing'an Range, NE China: the Tayuan example. Int. Geol. Rev. 61, 314–340.
Grove, T.L., Till, C.B., Krawczynski, M.J., 2012. The role of H_2O in subduction zone magmatism. Annu. Rev. Earth Pl. Sc. 40, 413–439.
Guo, F., Nakamura, E., Fan, W.M., Kobayoshi, K., Li, C.W., 2007. Generation of Paleocene adakitic andesites by magma mixing, Yanji area, NE China. J. Petrol. 48, 661–692.
Gutscher, M.A., Maury, F., Eissen, J.P., Bourdon, E., 2000. Can slab melting be caused by flat subduction? Geology 28, 535–538.
Hacker, B.R., Ratschbacher, L., Webb, L., McWilliams, M.O., Ireland, T., Calvert, A., Dong, S., Wenk, H.R., Chateigner, D., 2000. Exhumation of ultrahigh-pressure continental crust in east central China: Late Triassic-Early Jurassic tectonic unroofing. J. Geophys. Res.-Sol. Ea. 105, 13339–13364.
Hastie, A.R., Kerr, A.C., Pearce, J.A., Mitchell, S.F., 2007. Classification of altered volcanic island arc rocks using immobile trace elements: development of the Th–Co discrimination diagram. J. Petrol. 48, 2341–2357.
Hernlund, J.W., Tackley, P.J., Stevenson, D.J., 2008. Buoyant melting instabilities beneath extending lithosphere: 1. Numerical models. J. Geophys. Res. 113, B04405.
Hou, H.S., Wang, H.Y., Gao, R., Li, Q.S., Li, H.Q., Xiong, X.S., Li, W.H., Tong, Y., 2015. Fine crustal structure and deformation beneath the Great Xing'an Ranges, CAOB: Revealed by deep seismic reflection profile. J. Asian Earth Sci. 113, 491–500.
Houseman, G.A., Molnar, P., 1997. Gravitational (Rayleigh–Taylor) instability of a layer with non-linear viscosity and convective thinning of continental lithosphere. Geophys. J. Int. 128, 125–150.
Huang, B., Fu, D., Li, S., Ge, M., Zhou, W., 2016. The age and tectonic implications of the Hegenshan ophiolite in Inner Mongolia. Acta Petrol. Sin. 32, 158–176. in Chinese with English abstract.
Huang, X.L., Yu, Y., Li, J., Tong, L.X., Chen, L.L., 2013. Geochronology and petrogenesis of the early Paleozoic I-type granite in the Taishan area, South China: middle-lower crustal melting during orogenic collapse. Lithos 177, 268–284.
Imbgmr, 1991. Inner Mongolian Bureau of Geology Mineral Resources. In: Regional Geology of Inner Mongolia. Geological Publishing House, Beijing, pp. 1–725. in Chinese with English abstract.
Jahn, B.M., Capdevila, R., Liu, D., Vernon, A., Badarch, G., 2004. Sources of Phanerozoic granitoids in the transect Bayanhongor-Ulaan Baatar, Mongolia: geochemical and Nd isotopic evidence, and implications for Phanerozoic crustal growth. J. Asian Earth Sci. 23, 629–653.
Ji, Z., Ge, W.C., Yang, H., Tian, D.X., Chen, H.J., Zhang, Y.L., 2018. Late Carboniferous-Early Permian high- and low-Sr/Y granitoids of the Xing'an Block, northeastern China: implications for the late Paleozoic tectonic evolution of the eastern Central Asian Orogenic Belt. Lithos 322, 179–196.
Ji, Z., Meng, Q.A., Wan, C.B., Zhu, D.F., Ge, W.C., Yang, H., Zhang, Y.L., Dong, Y., 2019a. Geodynamic evolution of flat-slab subduction of Paleo-Pacific Plate: Constraints from Jurassic adakitic lavas in the Hailar Basin, NE China. Tectonics 38, 4301–4319.
Ji, Z., Meng, Q.A., Wan, C.B., Ge, W.C., Yang, H., Zhang, Y.L., Dong, Y., Jin, X., 2019b. Early Cretaceous adakitic lavas and A-type rhyolites in the Songliao Basin, NE China: implications for the mechanism of lithospheric extension. Gondwana Res. 71, 28–48.
Ji, Z., Zhang, Y.L., Wan, C.B., Ge, W.C., Yang, H., Dong, Y., Jing, Y., 2021. Recycling of crustal materials and implications for lithospheric thinning: Evidence from Mesozoic volcanic rocks in the Hailar-Tamtsag Basin. NE China. Geoscience Frontiers 12, 101184.
Jian, P., Kröner, A., Windley, B.F., Yuruo Shi, Y.R., Zhang, W., Zhang, L.Q., Yange, W.R., 2012. Carboniferous and Cretaceous mafic-ultramafic massifs in Inner Mongolia (China): a SHRIMP zircon and geochemical study of the previously presumed integral "Hegenshan ophiolite". Lithos 142–143, 48–66.
Jing, Y., Ge, W.C., Dong, Y., Yang, H., Bi, J.H., Zhou, H.Y., Xing, D.H., 2020. Early–middle Permian southward subduction of the eastern Paleo-Asian Ocean: Constraints from geochronology and geochemistry of intermediate–acidic volcanic rocks in the northern margin of the North China Craton. Lithos 364–365, 10549.
Jung, S., Hoernes, S., Mezger, K., 2002. Synorogenic melting of mafic lower crust: constraints from geochronology, petrology and Sr, Nd, Pb and O isotope geochemistry of quartz diorites (Damara orogen, Namibia). Contrib. Mineral. Petrol. 143, 551–566.
Kaislaniemi, L., van Hunen, J., Allen, M.B., Neill, I., 2014. Sublithospheric small-scale convection—a mechanism for collision zone magmatism. Geology 42, 291–294.
Kay, R.W., Kay, S.M., 1991. Creation and destruction of lower continental crust. Geol. Rundsch. 80, 259–278.
Kay, R.W., Kay, S.M., 1993. Delamination and Delamination Magmatism. Tectonophysics 219, 177–189.
Kepezhinskas, P., McDermott, F., Defant, M.J., Hochstaedter, A., Drummond, M.S., Hawkesworth, C.J., Koloskov, A., Maury, R.C., Bellon, H., 1997. Trace element and Sr–Nd–Pb isotopic constraints on a three-component model of Kamchatka Arc petrogenesis. Geochim. Cosmochim. Acta 61, 577–600.
Klemme, S., O'Neill, H.S.C., 2000. The near-solidus transition from garnet lherzolite to spinel lherzolite. Contrib. Miner. Petrol. 138, 237–248.
LaFlèche, M.R., Camire, G., Jenner, G.A., 1998. Geochemistry of post-Acadian, Carboniferous continental intraplate basalts from the Maritimes basin, Magdalen islands, Quebec, Canada. Chemical Geology 148, 115–136.
Li, J.Y., 2006. Permian geodynamic setting of Northeast China and adjacent regions: closure of the Paleo-Asian ocean and subduction of the Paleo-Pacific plate. J. Asian Earth Sci. 26, 207–224.
Li, Y., Xu, W.L., Wang, F., Tang, J., Pei, F.P., Wang, Z.J., 2014. Geochronology and geochemistry of late Paleozoic volcanic rocks on the western margin of the SongnenZhangguangcai Range Massif, NE China: implications for the amalgamation history of the Xing'an and Songnen-Zhangguangcai Range massifs. Lithos 205, 394–410.
Li, Y., Xu, W.L., Tang, J., Sun, C.Y., Zhang, X.M., Xiong, S., 2020. Late Paleozoic igneous rocks in the Xing'an Massif and its amalgamation with the Songnen Massif. NE China. J. Asian Earth Sci. 197, 104407.
Liao, J., Wang, Q., Gerya, T., Ballmer, M.D., 2017. Modeling craton destruction by hydration-induced weakening of the upper mantle. J. Geophys. Res. Solid Earth 122, 7449–7466.

Liu, Y.J., Li, W.M., Feng, Z.Q., Wen, Q.B., Neubauer, F., Liang, C.Y., 2017. A review of the Paleozoic tectonics in the eastern part of Central Asian Orogenic Belt. Gondwana Res. 43, 123–148.
Liu, Y.J., Feng, Z.Q., Jiang, L.W., Jin, W., Li, W.M., Guan, Q.B., Liang, C.Y., 2019. Ophiolite in the eastern Central Asian Orogenic Belt. NE China. Acta Petrol. Sin. 35, 3017–3047. in Chinese with English abstract.
Liu, Y.J., Li, W.M., Ma, Y.F., Feng, Z.Q., Guan, Q.B., Li, S.Z., Chen, Z.X., Liang, C.Y., Wen, Q.B., 2021. An orocline in the eastern Central Asian Orogenic Belt. Earth Sci. Rev. 221, 103808.
Lu, L., Qin, Y., Zhang, K.J., Han, C.Y., Wei, T., Li, Z.F., Qu, Z.H., 2020. Provenance and tectonic settings of the late Paleozoic sandstones in Central Inner Mongolia, NE China: Constraints on the evolution of the southeastern Central Asian Orogenic Belt. Gondwana Res. 77, 111–135.
Luan, J.P., Yu, J.J, Yu, J.L., Cui, Y.C., Xu, W.L., 2019. Early Neoproterozoic magmatism and the associated metamorphism in the Songnen Massif, NE China: Petrogenesis and tectonic implications. Precambrian Res. 328, 250–268.
Ma, L., Jiang, S.Y., Hofmann, A.W., Dai, B.Z., Hou, M.L., Zhao, K.D., Chen, L.H., Li, J.W., Jiang, Y.H., 2014. Lithospheric and asthenospheric sources of lamprophyres in the Jiaodong Peninsula: a consequence of rapid lithospheric thinning beneath the North China Craton? Geochim. Cosmochim. Acta 124, 250–271.
Ma, Y.F., Liu, Y.J., Wang, Y., Tang, Z., Qian, C., Qin, T., Feng, Z.Q., Sun, W., Zang, Y.Q., 2019. Geochronology and geochemistry of the Carboniferous felsic rocks in the central Great Xing'an Range, NE China: implications for the amalgamation history of Xing'an and Songliao-Xilinhot blocks. Geol. J. 54, 482–513.
Ma, Y.F., Liu, Y.J., Qin, T., Sun, W., Zang, Y.Q., Zhang, Y.J., 2020a. Late Devonian to early Carboniferous magmatism in the western Songliao-Xilinhot block, NE China: implications for eastward subduction of the Nenjiang oceanic lithosphere. Geol. J. 55, 2208–2231.
Ma, Y.F., Liu, Y.J., Wang, Y., Qin, T., Chen, H.J., Sun, W., Zang, Y.Q., 2020b. Late Carboniferous mafic to felsic intrusive rocks in the central Great Xing'an Range, NE China: petrogenesis and tectonic implications. Int. J. Earth Sci. 109, 761–783.
Ma, Q., Zheng, J.P., Xu, Y.G., Griffin, W.L., Zhang, R.S., 2015. Are continental "adakites" derived from thickened or foundered lower crust? Earth Planet. Sci. Lett. 419, 125–133.
Macera, P.M., Gasperini, D., Ranalli, G., Mahatsent, R., 2008. Slab detachment and mantle plume upwelling in subduction zones: an example from the Italian South-Eastern Alps. J. Geodyn. 45, 32–48.
Macpherson, C.G., Dreher, S.T., Thirlwall, M.F., 2006. Adakites without slab melting: high pressure differentiation of island arc magma, Mindanao, the Philippines. Earth Planet. Sci. Lett. 243, 581–593.
Martin, H., Smithies, R.H., Rapp, R., Moyen, J.F., Champion, D., 2005. An overview of adakite, tonalite–trondhjemite–granodiorite (TTG), and sanukitoid: relationships and some implications for crustal evolution. Lithos 79, 1–24.
McKenzie, D., O'Nions, R.K., 1991. Partial melt distributions from inversion of rare earth element concentrations. J. Petrol. 32, 1021–1091.
Meng, Q.A., Wan, C.B., Zhu, D.F., Zhang, Y.L., Ge, W.C., Wu, F.Y., 2013. Age assignment and geological significance of the "Budate Group" in the Hailar Basin. Sci. China Earth Sci. 56, 970–979.
Meschede, M., 1986. A method of discriminating between different types of mid-ocean ridge basalts and continental tholeiites with the Nb–Zr–Y diagram. Chem. Geol. 56, 207–218.
Miao, L.C., Liu, D.Y., Zhang, F.Q., Fan, W.M., Shi, Y.R., Xie, H.Q., 2007. Zircon SHRIMP U-Pb ages of the "Xinghuadukou Group" in Hanjiayuanzi and Xinlin areas and the "Zhalantun Group" in Inner Mongolia, Da Hinggan Mountains. Chin. Sci. Bull. 52, 1112–1124.
Miao, L.C., Fan, W.M., Liu, D.Y., Zhang, F.Q., Shi, Y.R., Guo, F., 2008. Geochronology and geochemistry of the Hegenshan ophiolitic complex: Implications for late-stage tectonic evolution of the Inner Mongolia-Daxinganling Orogenic Belt. China. J. Asian Earth Sci. 32, 348–370.
Mitchell, A.L., Grove, T.L., 2015. Melting the hydrous, subarc mantle: the origin of primitive andesites. Contrib. Miner. Petrol. 170, 1–23.
Moyen, J.F., 2009. High Sr/Y and La/Yb ratios: the meaning of the "adakitic signature". Lithos 112, 556–574.
Müntener, O., Kelemen, P.B., Grove, T.L., 2001. The role of H_2O during crystallisation of primitive arc magmas under uppermost mantle conditions and genesis of igneous pyroxenites: an experimental study. Contrib. Miner. Petrol. 141, 643–658.
O'Reilly, S.Y., Griffin, W.L., 2013. Mantle metasomatism. Metasomatism and the Chemical Transformation of Rock. Springer, Berlin Heidelberg, pp. 471–533.
Oh, J.I., Choi, S.H., Yi, K., 2016. Origin of adakite-like plutons in southern Korea. Lithos 262, 620–635.
Pearce, J.A., 2008. Geochemical fingerprinting of oceanic basalts with applications to ophiolite classification and the search for Archean oceanic crust. Lithos 100, 14–48.
Pei, F.P., Xu, W.L., Yang, D.B., Zhao, Q.G., Liu, X.M., Hu, Z.C., 2007. Zircon U–Pb geochronology of basement metamorphic rocks in the Songliao Basin. Chin. Sci. Bull. 52, 942–948.
Peslier, A.H., Woodland, A.B., Bell, D.R., Lazarov, M., Lapen, T.J., 2012. Metasomatic control of water contents in the Kaapvaal cratonic mantle. Geochim. Cosmochim. Acta 97, 213–246.
Pichavant, M., Macdonald, R., 2007. Crystallization of primitive basaltic magmas at crustal pressures and genesis of the calcalkaline igneous suite: experimental evidence from St Vincent, Lesser Antilles arc. Contrib. Miner. Petrol. 154, 535–558.
Plank, T., Langmuir, C.H., 1998. The chemical composition of subducting sediment and its consequences for the crust and mantle. Chem. Geol. 145, 325–394.
Prelević, D., Akal, C., Romer, R.L., Mertz-Kraus, R., Helvacı, C., 2015. Magmatic response to slab tearing: constraints from the Afyon Alkaline Volcanic Complex, Western Turkey. J. Petrol. 56, 527–562.
Qian, C., Chen, H.J., Lu, L., Pang, X.J., Qin, T., Wang, Y., 2018. The discovery of Neoarchean granite inLongjiang area, Heilongjiang Province. Acta Geol. Sin. 39, 27–36.
Qian, Q., Hermann, J., 2013. Partial melting of lower crust at 10–15 kbar: constraints on adakite and TTG formation. Contrib. Mineral. Petrol. 165, 1195–1224.
Rapp, R.P., Watson, E.B., 1995. Dehydration melting of metabasalt at 8–32 kbar: implications for continental growth and crust-mantle recycling. J. Petrol. 36, 891–931.
Rapp, R.P., Shimizu, N., Norman, M.D., Applegate, G.S., 1999. Reaction between slabderived melts and peridotite in the mantle wedge: experimental constraints at 3.8 GPa. Chem. Geol. 160, 335–356.
Reubi, O., Blundy, J., 2009. A dearth of intermediate melts at subduction zone volcanoes and the petrogenesis of arc andesites. Nature 461, 1269–1274.
Ridolfi, F., Renzulli, A., Puerini, M., 2010. Stability and chemical equilibrium of amphibole in calc-alkaline magmas: an overview, new thermobarometric formulations and application to subduction-related volcanoes. Contrib. Miner. Petrol. 160, 45–66.
Rollinson, H.R., 1993. Using geochemical data: evaluation, presentation, interpretation. Longman Singapore Publishers (Pte) Ltd., Singapore, pp. 1–352.
Saunders, A. D., Storey, M., Kent, R. W., Norry, M. J., 1992. Consequences of plume lithosphere interactions. In: Storey, B.C., Alabaster, T., Pankhurst, R.J. (Eds.), Magmatism and the Cause of Continental Break-Up. Geol. Soc. Spec. Publ, Lond., pp. 41–60.
Rosenbaum, G., Gasparon, M., Lucente, F.P., Peccerillo, A., Miller, M.S., 2008. Kinematics ofslab tear faults during subduction segmentation and implicationsfor Italian magmatism. Tectonics 27, TC2008.
Sengör, A.M.C., Natal'in, B.A., Burtman, V.S., 1993. Evolution of the Altaid tectonic collage and Palaeozoic crustal growth in Eurasia. Nature 364, 299–307.
Sharma, M., 1997. Siberian traps. In: Mahoney, J.J., Coffin, M.F. (Eds.), Large Igneous Provinces: Continental, Oceanic, and Planetary Flood Volcanism, 100. American Geophysical Union Geophysical Monograph, pp. 273–295.
Soesoo, A., Bons, P.D., Gray, D.R., Foster, D.A., 1997. Divergent double subduction: tectonic and petrologic consequences. Geology 25, 755–758.
Song, S., Wang, M., Wang, C., Niu, Y., 2015a. Magmatism during continental collision, subduction, exhumation and mountain collapse in collisional orogenic belts and continental net growth: a perspective. Sci. China Earth Sci. 58, 1284–1304.
Song, S.G., Wang, M.M., Xu, X., Wang, C., Niu, Y.L., Allen, M.B., Su, L., 2015b. Ophiolites in the Xing'an-Inner Mongolia accretionary belt of the CAOB: implications for two cycles of seafloor spreading and accretionary orogenic events. Tectonics 34, 2221–2245.
Straub, S.M., 2003. The evolution of the Izu Bonin-Mariana volcanic arcs (NW Pacific) in terms of major element chemistry. Geochem. Geophys, Geosyst, p. 4.
Streck, M.J., Leeman, W.P., Chesley, J., 2007. High-magnesian andesite from Mount Shasta: a product of magma mixing and contamination, not a primitive mantle melt. Geology 35, 351–354.
Su, Y.Z., 1996. Paleozoic stratigraphy of Xing'an stratigraphical province. Jilin Geol. 15, 23–34. in Chinese with English abstract.
Sun, S.S., McDonough, W.F., 1989. Chemical and isotopic systematics of oceanic basalts: Implications for mantle composition and processes. In: Saunders, A.D., Norry, M.J. (Eds.), Magmatism in Ocean Basins. Publ, London, Geol. Soc. Spec, pp. 313–345.
Sun, D.Y., Wu, F.Y., Li, H.M., Lin, Q., 2000. Emplacement age of the post-orogenic A-type granites in Northwestern Lesser Xing'an Range, and its relationship to the eastward extension of Suolushan–Hegenshan–Zhalaite collisional suture zone. Chin. Sci. Bull. 45, 2217–2222. in Chinese with English abstract.
Tang, K.D., 1990. Tectonic development of Palaeozoic fold belts at the north margin of the Sino-Korean Craton. Tectonics 9, 249–260.
Tang, J., Xu, W.L., Wang, F., Wang, W., Xu, M.J., Zhang, Y.H., 2013. Geochronology and geochemistry of Neoproterozoic magmatism in the Erguna Massif, NE China: petrogenesis and implications for the breakup of the Rodinia supercontinent. Precambrian Res. 224, 597–611.
Turner, S., Arnaud, N., Liu, J., Rogers, N., Hawkesworth, C., Harris, N., Kelley, S., van Calsteren, P., Deng, W.M., 1996. Postcollisional, shoshonitic volcanism on the Tibetan plateau: implications for convective thinning of the lithosphere and the source of ocean island basalts. J. Petrol. 37, 45–71.
Wang, Q., 2010. A review of water contents and ductile deformation mechanisms of olivine: Implications for the lithosphere-asthenosphere boundary of continents. Lithos 120, 30–41.
Wang, Y., Fu, J.Y., Na, F.C., Liu, Y.C., Zhang, G.Y., Kang, Z., Yang, F., 2013. Geochemical characteristics and zircon U-Pb age of the gabbro-diorite in Jalaid Banner of Inner Mongolia and their geological significance. Geological Bulletin of China 32, 1525–1535.
Wang, Q., Xu, J.F., Jian, P., Bao, Z.W., Zhao, Z.H., Li, C.F., Xiong, X.L., Ma, J.L., 2006. Petrogenesis of adakitic porphyries in an extensional tectonic setting, Dexing, South China: implications for the genesis of porphyry copper mineralization. J. Petrol. 47, 119–144.
Wang, Q., Wyman, D.A., Xu, J., Dong, Y., Vasconcelos, P.M., Pearson, N., Wan, Y., Dong, H., Li, C., Yu, Y., Zhu, T., Feng, X., Zhang, Q., Zi, F., Chu, Z., 2008. Eocene melting of subducting continental crust and early uplifting of Central Tibet: evidence from central-western Qiangtang high-K calc-alkaline andesites, dacites and rhyolites. Earth Planet. Sci. Lett. 272, 158–171.
Wilson, M., 1989, Igneous Petrogenesis: London, Chapman & Hall, pp. 466 .

Winchester, J.A., Floyd, P.A., 1976. Geochemical magma type discrimination: Application to altered and metamorphosed basic igneous rocks. Earth Planet. Sci. Lett. 28, 459–469.
Windley, B.F., Alexeiev, D., Xiao, W.J., Kröner, A., Badarch, G., 2007. Tectonic models for accretion of the Central Asian Orogenic Belt. J. Geol. Soc. Lond. 164, 31–47.
Wood, D.A., 1980. The application of a Th-Hf-Ta diagram to problems of tectonomagmatic classification and to establishing the nature of crustal contamination of basaltic lavas of the British Tertiary Volcanic Province. Earth Planet. Sci. Lett. 50, 11–30.
Wu, F.Y., Sun, D.Y., Li, H.M., Wang, X.L., 2001. The nature of basement beneath the Songliao Basin in NE China: geochemical and isotopic constraints. Phys. Chem. Earth (Part A) 26, 793–803.
Wu, F.Y., Sun, D.Y., Li, H.M., Jahn, B.M., Wilde, S.A., 2002. A-type granites in northeastern China: age and geochemical constraints on their petrogenesis. Chem. Geol. 187, 143–173.
Wu, F.Y., Sun, D.Y., Ge, W.C., Zhang, Y.B., Grant, M.L., Wilde, S.A., Jahn, B.M., 2011. Geochronology of the Phanerozoic granitoids in Northeastern China. J. Asian Earth Sci. 41, 1–30.
Xiao, W.J., Santosh, M., 2014. The western Central Asian Orogenic Belt: a window to accretionary orogenesis and continental growth. Gondwana Res. 25, 1429–1444.
Xiao, W.J., Song, D.F., Windley, B.F., Li, J., Han, C., Wan, B., Zhang, J.E., Ao, S.J., Zhang, Z., 2020. Accretionary processes and metallogenesis of the Central AsianOrogenic Belt: advances and perspectives. Sci. China Earth Sci. 63, 329–361.
Xiao, W.J., Windley, B.F., Hao, J., Zhai, M.G., 2003. Accretion leading to collision and the Permian Solonker suture, Inner Mongolia, China: termination of the Central Asian orogenic belt. Tectonics 22, 1–20.
Xu, J.F., Shinjo, R., Defant, M.J., Wang, Q., Rapp, P.T., 2002. Origin of Mesozoic adakitic intrusive rocks in the Ningzhen area of East China: partial melting of delaminated lower continental crust? Geology 30, 1111–1114.
Xu, B., Zhao, P., Wang, Y.Y., Liao, W., Luo, Z.W., Bao, Q.Z., Zhou, Y.H., 2015. The preDevonian tectonic framework of Xing'an-Mongolia orogenic belt (XMOB) in north China. J. Asian Earth Sci. 97, 183–196.
Yang, H., Ge, W.C., Ji, Z., Yu, Q., Tian, D.X., 2019. Late Carboniferous to early Permian subduction-related intrusive rocks from the Huolongmen region in the Xing'an Block, NE China: new insight into evolution of the Nenjiang-Heihe suture. Int. Geol. Rev. 61, 1071–1104.
Yang, J.H., Wu, F.Y., Shao, J.A., Wilde, S.A., Xie, L.W., Liu, X.M., 2006. Constrains on the timing of uplift of the Yanshan Fold and Thrust Belt, north China. Earth Planet. Sci. Lett. 246, 336–352.
Yin, J.Y., Chen, W., Xiao, W.J., Yuan, C., Windley, B.F., Yu, S., Cai, K.D., 2017. Late Silurian–early Devonian adakitic granodiorite, A-type and I-type granites in NW Junggar, NW China: partial melting of mafic lower crust and implications for slab roll-back. Gondwana Research 43, 55–73.
Yin, A., Harrison, T.M., 2000. Geologic evolution of the Himalayan-Tibetan orogen. Annu. Rev. Earth Pl. Sc. 28, 211–280.
Yogodzinski, G.M., Kay, R.W., Volynets, O.N., Koloskov, A.V., Kay, S.M., 1995. Magnesian andesite in the western Aleutian Komandorsky region: implications for slab melting and processes in the mantle wedge. Geol. Soc. Am. Bull. 107, 505–519.
Yu, Q., 2017. Petrogenesis of the Late Paleozoic-Early Mesozoic intrusive rocks in the Xing'an terrane, and its geological implication. Ph.D. thesis. Jilin University.
Yu, Q., Ge, W.C., Zhang, J., Zhao, G.C., Zhang, Y.L., Yang, H., 2017. Geochronology, petrogenesis and tectonic implication of Late Paleozoic volcanic rocks from the Dashizhai Formation in Inner Mongolia. NE China. Gondwana Res. 43, 164–177.
Zhang, D. H., Huang, B. F., Meert, J. G., Zhao, G. C., Zhao, J., Zhao, Q., 2021. Micro-blocks in NE Asia amalgamated into the unified Amuria block by ~300 Ma: First paleomagnetic evidence from the Songliao block, NE China. J. Geophys. Res.-Sol. Ea. 126, e2021JB022881.
Zhang, F.Q., Chen, H.L., Cao, R.C., Meng, Q.A., Zhu, D.F., Wang, G.Z., 2010. Discovery of LatePaleozoic adakite from the basement of the Hailaer basin in NE China and its geological implication. Acta Petrol. Sin. 26, 633–641.
Zhang, Z.C., Li, K., Li, J.F., Tang, W.H., Chen, Y., Luo, Z.W., 2015. Geochronology and geochemistry of the Eastern Erenhot ophiolitic complex: Implications for the tectonic evolution of the Inner Mongolia-Daxinganling Orogenic Belt. J. Asian Earth Sci. 97, 279–293.
Zhang, Y., Pei, F.P., Wang, Z.W., Xu, W.L., Li, Y., Wang, F., Zhou, Z.B., 2018. Late Paleozoic tectonic evolution of the central Great Xing'an Range, northeast China: geochronological and geochemical evidence from igneous rocks. Geol. J. 53, 282–303.
Zhang, Y.J., Wu, X.W., Yang, Y.J., Cui, T.R., Jiang, B., Gou, W., Zhang, C., Qiang, C., Chen, H.J., Li, W., Li, L.C., Si, Q.L., 2016. Discovery and geological significance of adakitic rocks inthe Late Paleozoic Gegenaobao Formation in Zhalantun area, Middle DaxinganlingMountains. Geol. Resour., 227–236
Zhao, G.C., 2015. Jiangnan Orogen in South China: developing from divergent double subduction. Gondwana Res. 27, 1173–1180.
Zhao, P., Chen, Y., Xu, B., Faure, M., Shi, G., Choulet, F., 2013. Did the Paleo-Asian Ocean between North China Block and Mongolia Block exist during the late Paleozoic? First paleomagnetic evidence from central-eastern Inner Mongolia. China. J. Geophys. Res.-Sol. Ea. 118, 1873–1894.
Zhao, Z., Chi, X.G., Liu, J.F., Wang, T.F., Hu, Z.C., 2010. Late Paleozoic arc-related magmatism in Yakeshi region, Inner Mongolia: chronological and geochemical evidence. Acta Petrol. Sin. 26, 3245–3258. in Chinese with English abstract.
Zheng, Y.F., 2019. Subduction zone geochemistry. Geosci. Front. 10, 1223–1254.
Zheng, Y.F., Fu, B., Gong, B., Li, L., 2003. Stable isotope geochemistry of ultrahigh pressure metamorphic rocks from the Dabie-Sulu orogen in China: implications for geodynamics and fluid regime. Earth Sci. Rev. 62, 105–161.
Zhou, J.B., Han, J., Zhao, G.C., Zhang, X.Z., Cao, J.L., Wang, B., Pei, S.H., 2015. The emplacement time of the Hegenshan ophiolite: Constraints from the unconformably overlying Paleozoic strata. Tectonophysics 662, 398–415.
Zhou, J.B., Li, L., 2017. The Mesozoic accretionary complex in Northeast China: Evidence for the accretion history of Paleo-Pacific subduction. J. Asian Earth Sci. 145, 91–100.
Zhou, J.B., Wilde, S.A., Zhao, G.C., Han, J., 2018. Nature and assembly of microcontinental blocks within the paleo-Asian ocean. Earth Sci. Rev. 186, 76–93.
Zhou, C.Y., Wu, F.Y., Ge, W.C., Sun, D.Y., Abdel Rahman, A.A., Zhang, J.H., Cheng, R.Y., 2005. Age, geochemistry and petrogenesis of the cumulate gabbro in Tahe, northern Great Xing'an Range. Acta Petrol. Sin. 21, 763–775. in Chinese with English abstract.
Zhu, D.C., Wang, Q., Zhao, Z.D., Chung, S.L., Cawood, P.A., Niu, Y.L., Liu, S.A., Wu, F.Y., Mo, X.X., 2015. Magmatic record of India-Asia collision. Sci. Rep. 5, 14289.
Zhu, D.C., Li, S.M., Cawood, P.A., Wang, Q., Zhao, Z.D., Liu, S.A., Wang, L.Q., 2016. Assembly of the Lhasa and Qiangtang terranes in central Tibet by divergent double subduction. Lithos 245, 7–17.